Population and evolutionary dynamics during microbial range expansions

by

Saurabh Rajendra Gandhi

B.Tech., Indian Institute of Technology, Bombay (2013)

Submitted to the Department of Physics
in partial fulfillment of the requirements for the degree of

Doctor of Philosophy

at the

MASSACHUSETTS INSTITUTE OF TECHNOLOGY

February 2019

© Massachusetts Institute of Technology 2019. All rights reserved.

Author . . . .
Department of Physics
January 18, 2019

Certified by . . . .
Jeff Gore
Associate Professor
Thesis Supervisor

Accepted by . . . .
Nergis Mavalvala
Associate Department Head, Physics

Population and evolutionary dynamics during microbial range expansions

by

Saurabh Rajendra Gandhi

Submitted to the Department of Physics
on January 18, 2019, in partial fulfillment of the
requirements for the degree of
Doctor of Philosophy

Abstract

Spatial expansions occur across multiple scales, from the expanding range of a species to the growth of tumors and microbial biofilms. In ecology, range expansions are becoming more frequent due to environmental changes and rare long distance dispersal, often facilitated by anthropogenic activities. Simple models in theoretical ecology explain many emergent properties of range expansions, such as a constant expansion velocity, in terms of organism-level properties such as growth and dispersal rates. Moreover, the evolution and potentially even the survival of an expanding population depends on its genetic diversity, which is also predicted to reduce drastically during range expansions. However, testing these quantitative predictions in natural populations is difficult because of large environmental variability and the inability of replicating historical processes. In this thesis, I describe the use of a microbial model system to gain a deeper understanding of spatial range expansions in a controlled and replicable setting. In particularly, I study the role of cooperative growth in spatial expansions. Given the prevalence of cooperative growth in nature, understanding the effects of cooperativity is essential to managing invading species and understanding their evolution. For non-cooperative growth, the expansion dynamics are dominated by population growth at the low-density front, which pulls the expansion forward. I find these expansions to be in close quantitative agreement with the classical theory of pulled waves by Fisher and Skellam, suitably adapted to my experimental system. However, as cooperativity increases, the expansions transition to being pushed, i.e. controlled by growth in the bulk as well as in the front. In addition to the population dynamics, cooperation within populations is also predicted to significantly alter the evolutionary fate of expanding populations. This difference in evolutionary dynamics within pulled and pushed waves is also studied experimentally.

Thesis Supervisor: Jeff Gore
Title: Associate Professor

Acknowledgments

Firstly, I thank my Ph.D advisor, Prof. Jeff Gore, for his excellent mentorship, and continued support and guidance throughout my time at MIT. I also thank Prof. Kirill Korolev for his immense inputs in guiding the design and execution of this study, as well as my other advisors, Prof. Mehran Kardar (my academic advisor), Prof. Ibrahim Cisse and Prof. Nuh Gedik (my thesis committee members). I am grateful for the contribution of my collaborator, Dr. Eugene Yurtsev, in designing the experiments as well as teaching me wet lab techniques at the very beginning when I had no prior experience with microbiology. I am also grateful for the insights and help provided by my labmates, Clare Abreau, Daniel Amor, Tatiana Artemova, Kevin Axelrod, Tommaso Biancalani, Martina Dal Bello, Hasan Celiker, Arolyn Conwill, Lei Dai, Manoshi Datta, Alfonso Perez Escudero, Jonathan Friedman, Shreyas Gokhale, Dave Healey, Logan Higgins, Anthony Ortiz, Sivan Pearl, Christoph Ratzke, Longzhi Tan, Mendeli Vainstein, Andrea Velenich, Nicole Vega and Avihu Yona. I also thank the support staff that made my work possible, including the lab manager, Olutayo (Ty) Ogun, lab administrative assistants Monica Wolf, Kerry Forristall and Natalie Adams and the Physics department staff, Cathy Modica and Sydney Miller.

Contents

1 Introduction 15

2 Range expansions transition from pulled to pushed waves with increasing cooperation 21

2.1 Significance statement 21
2.2 Introduction 22
2.3 Results 25
  2.3.1 Experimental system 25
  2.3.2 Testing the theory of pulled waves 27
  2.3.3 Expansions transition from pulled to pushed as cooperativity increases 28
2.4 Discussion 31

3 Cooperation mitigates diversity loss during microbial range expansions 39

3.1 Significance statement 39
3.2 Introduction 39
3.3 Results 42
  3.3.1 Loss of diversity during expansions 43
  3.3.2 Effective population size is correlated to the ‘pushedness’ of expansion wave 44
  3.3.3 Distinguishing selective sweeps from jackpots 46
3.4 Discussion 47

A Appendix to chapter 2 **55**

A.1 Materials and methods 55

A.1.1 Strains 55

A.1.2 Experimental protocols 55

A.2 Reaction-diffusion models for one-dimensional range expansions . . . 56

A.3 Expansions in discrete space and time models 58

A.4 Cubic model of the Allee effect 60

A.5 A mechanistic growth model captures the Allee effect and shows a transition from pulled to pushed waves with increasing sucrose 61

A.6 Simulations 65

A.7 Supplementary figures 66

B Appendix to chapter 3 **83**

B.1 Materials and methods 83

B.1.1 Growth rate measurements and calculation of Fisher velocities 83

B.1.2 Expansion experiment protocols 84

B.1.3 Definition of front 84

B.2 Supplementary figures 85

List of Figures

2-1 Theoretical predictions for the velocity and spatial density profile of pulled and pushed waves were quantitatively tested in metapopulations of budding yeast, *S. cerevisae*, in a controlled experimental setup. . . 33

2-2 In pulled waves, expansion velocity depends on the growth rate only at low densities irrespective of the carrying capacity. 34

2-3 For pulled waves, the growth rate at low density is sufficient to determine the emergent wave properties quantitatively. Over a wide range of environmental conditions, the observed expansion velocities and the spatial decay rates (SDR) of the population density at the front closely match the predictions based on the measured low-density growth rate. 35

2-4 Expansions transition from pulled to pushed at an intermediate strength of Allee effect within the weak regime. 36

2-5 A sufficiently large Allee effect gives rise to pushed waves that can be identified based on their deviations from predictions based on linearized growth. 38

3-1 Yeast expanding in a 1D metapopulation landscape is used to study the genetic consequences of pulled and pushed range expansions. . . . 50

3-2 Yeast expanding in different growth media loses diversity at very different rates even though the wavefronts have similar physical properties, such as velocity and bulk density 51

3-3 The ratio of observed velocity to the Fisher velocity (defined as the pushedness) determines the rate of diversity loss during expansions . 52

3-4 Rapid takeover of the front population by one of the genotypes caused by rare fluctuations of the front can be distinguished from selective sweeps based on the trajectory in the front width - velocity state space 54

A-1 When populations grow logistically, Fisher's equation predicts traveling waves of constant velocity, with an exponential spatial profile near the front. Both of these emergent properties depend only on the low-density growth rate, and are independent of the carrying capacity. . . 67

A-2 The maximal per capita growth rate in galactose (a) and glucose (b) never significantly exceeds the per capita growth rate at low density. . 68

A-3 Effect of discretizing space and time (and addition of demographic stochasticity) on predicted velocity in glucose (a), galactose (b) and sucrose (c) environments. 69

A-4 Demographic stochasticity significantly affects the spatial decay rate at the front. 70

A-5 Low density growth rate increases slowly with increasing sucrose concentration 71

A-6 Magnitude of Allee effect increases with increasing sucrose concentration. 72

A-7 A mechanistic model of yeast growth on sucrose and glucose predicts a transition from pulled to pushed waves (Section A.5) 73

A-8 A mechanistic model for growth on glucose and sucrose predicts velocities close to what are observed experimentally 74

A-9 Fitting the yield parameter in the mechanistic growth model 75

A-10 Low density growth rate measurement in different media 76

A-11 Model predictions of low density growth rates for different sucrose concentrations 77

A-12 Distribution of fitted parameter values 78

A-13 Mechanistic model fits for different sucrose concentrations 79

A-14 Overview of the mechanistic model and simulations 80

B-1 Density dependence of growth and fits for low density growth rate for different strain-media combinations 86
B-2 Jackpots in experiments 87
B-3 All evolution state space diagrams 88
B-4 Front diffusion figure 89

List of Tables

A.1 Fit parameters for mechanistic growth model of *S. Cerevisiae* on glucose and sucrose 81

B.1 Growth rates and Fisher velocities of yeast strains in different growth media 90

Chapter 1

Introduction

Physically one of the largest in size in the world, the Cane toad is a species of toad that is native to southern and mainland central America. It derives its name from the function it plays in controlling pests that afflict sugarcane crops in this region. For this reason, between 1935 to 1937, approximately 60,000 individuals of this toad, taken from Hawaii, were introduced in Queensland in northeastern Australia, in an attempt to control local pests, the grey-backed cane beetle (*Dermolepida albohirtum*) and French's beetle (*Lepidiota frenchi*). While the toads took very well to the new territory, it turned out that they were not at all effective against these particular pests. However, without the natural predators and competitors of the toad from their native ecosystem, their population in Australia exploded, and they rapidly spread across the continent. The toads have a poisonous skin, causing the death of their Australian predators, thus affecting the food chain, and hence the entire ecology of the region. Today, their population in Australia is estimated to be over 1.5 billion, and they continue to expand their territory by 50 to 60 kilometers every year [1, 2, 3]. Moreover, they have been found to evolve longer legs over time, resulting in an accelerating expansion, subjecting ever larger areas to extensive environmental, social, health and economic damage.

In a similar turn of events, the Gypsy moth was brought to the US from its native Europe in 1869 with the intention of breeding it for silk production. It was released into the wild, this time by accident, in Medford, Massachusetts, and now extends its range all the way to Wisconsin in central US. This invasive pest has caused defoliation of millions of hectares of forests, once again causing extensive environmental and economic damage estimated at billions of dollars. Without any intervention, it has been found to expand on average at the rate of about 20 km/year, but unlike the toads, the expansion speed of the moths hasn't undergone any evolution. Curiously, however, the expansion speed is not constant, but oscillates, so that the geographical range of the moths increases approximately every alternate year and stays stable during the intervening time [4, 5, 6].

Over the past few decades, invasive species have been introduced around the world at an increasing rate because of increase in trade and travel [7]. Although it initially takes time for the invaders to adapt to and establish in the new area, they also do not have to face their native predators and competitors. Consequently, once established, they often outcompete local species, resulting in extensive (and usually detrimental) reorganization of the local ecology. Extensive studies of specific invaders as well as a good general understanding of the dynamics of spatial expansion is critical for devising strategies to control and mitigate such biological invasions.

Even without invaders, species undergo range shifts and range expansions naturally in response to changing climate and environmental conditions. For instance, in the past, repopulations from small geographical reserves into extensive areas have occurred on a global scale following ice ages [8, 9, 10]. The survival of the species during such large scale repopulations depends on their ability to adapt and, as in the case of the toads, evolve during the expansion, which in turn depends on the availability of a diverse genetic pool within the population. The very process of expansion, however, also erodes genetic diversity because every time the population advances into a new territory, it does so by establishing a small subpopulation of founders (carrying only part of the total gene pool), which then grows to occupy the territory. Thus, along with the population dynamics, it is also necessary to understand evolutionary dynamics during expansions to successfully predict the establishment, survival and expansion rates of species.

Spatial population expansions occur at multiple length and time scales, including the growth of bacterial biofilms, growth of tumors, and the spread of infectious diseases. General principles connecting the demographic properties of individuals within the populations, such as the growth and dispersal rate, to the emergent properties of the expansion wave in one system can potentially shed light on a broad range of other systems. For instance, cells in tumors have been shown to have a very high genetic diversity, and undergo non-darwinian evolution (i.e. evolution is not driven by fitness, so that even individuals with a lower fitness survive and proliferate) [11]. A similar phenomenon of non-Darwinian evolution has been observed in the ecological and microbial expansion contexts where the expansion causes the continued proliferation of even deleterious mutations in the population [12]. Since it is easier to manipulate and observe bacterial cells compared to mammalian ones, a reasonable approach to further our understanding of the genetics of tumors might be to tease apart the mechanisms behind non-darwinian selection in bacterial expansions.

Given their small size and generation time, microbial populations are often used in ‘microcosm experiments’, where eco-evolutionary phenomena can be studied in a much more controlled and replicable setting over shorter time scales (days to months) compared to ecological field studies (that might take years or decades and are subject to large environmental fluctuations that often confound the results). While this approach trades off some potentially relevant complexities of real ecosystems, it adds biological realism and has been successfully employed in the past to bridge the gap between theory and field observations. For instance, ecosystems often show multiple stable states, such as a healthy and a eutrophic lake, and ecologists are interested in predicting how much fertilizer the lake can absorb before transitioning into the unhealthy state. Microcosm experiments with yeast have been used to demonstrate how the critical slowing down of dynamics near the bifurcation point of a dynamical system can be used to predict such an ecological state transition under deteriorating environmental conditions [13]. In the same spirit, my research has been focused on using a microbial system to observe some interesting phenomena that occur during the spatial expansion of populations. In particular, considerable effort has been put into understanding how cooperative behaviour within a population alters its expansion and evolutionary dynamics, and I test some of these predictions using yeast as a model organism.

When growing in the presence of finite resources, the per capita availability of resources decreases with increasing population density, and as a result, so does the per capita growth rate. Thus, in general, it is assumed that a species will grow fastest in the limit of zero density, and the per capita growth rate decreases monotonically with increasing density. However, the growth rate of a species at very low densities can be subdued due to numerous reasons - in a larger group the individuals may better survive predators, hunt more effectively, or find mates more easily. In such populations, there is a range of densities over which the growth rate depends positively on the density, and such populations are said to grow cooperatively. In contrast, populations that do not display this subdued growth at low densities are said to grow competitively.

In the presence of simple diffusive dispersal, it has been long known that competitively growing populations expand at a constant velocity. Moreover, the local growth rate of such populations is the highest at the very tip of the expanding front (which is at the lowest density), and the expansion velocity of these populations depends on the single growth parameter, the growth rate at the low density tip. Cooperation is predicted to add numerous interesting features to this simple picture. First of all, since growth is now fastest in the interior of the population rather than the expanding tip, the velocity dependence on growth is much more complex. Moreover, in the presence of a spatially structured environment, cooperation is predicted to cause effects such as the pulsed expansion that was seen empirically in the Gypsy moths, invasion pinning (where over an extended range of parameters like the diffusion rate, the expanding front is pinned and does not move) [14, 15], velocity locking (where the velocity of the front becomes insensitive to changing parameters) and in some cases, even negative velocities (where the population remains stable in the absence of dispersal, but by adding dispersal, the population actually contracts rather than expand). Besides the rich phenomenology at the population level, cooperation is also predicted to dramatically alter the dynamics of evolution during expansion.

In the microcosm experiments that we have developed, yeast expands in a structured landscape consisting of discrete patches of space, where we have precise control over dispersal between patches. By changing the growth medium of the yeast, we can also tune the amount of cooperation within the yeast populations. This combination allows us to quantitatively examine some of the aforementioned theoretical predictions. In the following two chapters, I describe how we use this system to first characterize the differences in expansion dynamics with and without cooperation; and then go on to examine the consequences of these differences on the evolutionary fate of these expansions.

Chapter 2

Range expansions transition from pulled to pushed waves with increasing cooperation

This chapter was published in similar form in [16]. This work was done in collaboration with Eugene Yurtsev and Prof. Kirill Korolev.

2.1 Significance statement

Species undergo range shifts in response to changing climate or following an introduction to a new environment. Invasions often incur significant economic cost and threaten biodiversity. Ecological theory predicts two distinct types of expansion waves: pulled and pushed, depending on the degree of cooperativity in the population. Although pulled and pushed invasions differ dramatically in how population-level properties such as the expansion rate depend on the organism-level properties such as rates of growth and dispersal, these theoretical predictions have not been tested empirically. Here, we use a microbial model system to perform these tests and demonstrate that pulled and pushed waves can be distinguished based on their dynamics.

2.2 Introduction

From a local disturbance by an invasive species to the global expansion of the biosphere after an ice age, range expansions have been a major ecological and evolutionary force [8, 17]. Range expansions and range shifts are becoming increasingly frequent due to the deliberate introduction of foreign species [3, 18], unintentional introductions caused by global shipping [7], and temperature changes associated with climate change [19, 20]. Many invasions disturb ecosystem functions, reduce biodiversity, and impose significant economic costs [21, 22]. The interest in invasion forecasting and management resulted in a substantial effort to develop predictive mathematical models of range expansions [18, 4, 23, 24, 25], but empirical tests of these models have been less extensive.

Species invade new territory through a combination of dispersal and local growth. Mathematically, these dynamics can be described by a variety of models depending on the details of the species ecology or simplifying assumptions [26]. For example, the invasion of house finches in North America has been successfully modeled with integrodifference equations [18]. Continuous reaction-diffusion equations have been used to describe the expansion of trees following the end of an ice age and the expansion of musk rats form central Europe [27], while metapopulation models with disjoint patches of suitable habitat and discrete generations are more appropriate for certain butterflies living in temperate climate [28]. One of the great achievements of mathematical ecology is the discovery that all these diverse models of population expansion can be divided into two broad classes of pulled and pushed expansion with very different properties.

The class of the expansion is determined by how the per capita growth rate depends on population density [29, 30]. While some populations experience only intraspecific competition and grow best at very low densities, others exhibit an Allee effect and grow best at intermediate densities, due to intraspecific facilitation, higher chances of finding mates, or other factors [31, 32, 33, 34]. These Allee effects may be weak (reduced but positive growth rate at low density) or strong (inability to survive at low density). Pulled expansions occur when Allee effects are small, and the expansion velocity depends only on the growth rate at low densities and the rate of dispersal. Such expansions are dominated by the dynamics at the very edge of the expanding wave front, which effectively pulls the wave forward [29, 30, 35]. As a result, pulled invasions are known to be sensitive to demographic fluctuations and lead to rapid loss of genetic diversity because the population size at the expansion edge is very small [36, 37, 38, 39, 40]. When the Allee effect is more severe, including but not restricted to the case of strong Allee effects, the expansions are pushed. In contrast to the simple and universal theory of pulled expansions, the velocity and other properties of pushed expansions depend on the per capita growth rate at all population densities, and thus, are sensitive to all the details of the species ecology [29, 30, 35].

Since direct observations of the Allee effect are often challenging, it is important to find alternative ways to distinguish pulled and pushed expansions. Unfortunately, these two invasion classes share many generic properties. In particular, both expansions advance as population waves that move at constant velocity and maintain a constant shape of the expansion front. Even the qualitative shape of the expansion front is the same for pulled and pushed waves because population densities decay exponentially at the expansion edge in both cases [29, 30]. Thus, one needs quantitative rather than qualitative comparison between theory and observations to distinguish pulled and pushed waves.

Although high quality quantitative data on range expansions is often limited, several studies have successfully tested theories of range expansions in natural and laboratory populations. Veit and Lewis could accurately describe the spread of house finches in North America by incorporating an Allee effect and long-distance dispersal [18]. Importantly, this was one of the early studies highlighting the difference between pulled and pushed invasions. Lewis and Kareiva later showed that the rate of spread also depends on the initial spatial abundance profile of the invader [41]. Melbourne and Hastings have carried out a very detailed comparison between theory and experiment for a laboratory population of flour beetles and showed that the unavoidable heterogeneity of the founding organisms leads to large variation in the rate of spread between replica populations [42]. At the microscopic scale, Wakita tested the expected relation between the rate of spread and nutrient availability in E. coli [43] and Giometto et. al. used the theory of pulled waves to describe the expansion of tetrahymena in linear channels [44]. All of these studies however focused only on the rate of invasion and did not test theoretical predictions for the shape of the invading fronts. More importantly, these studies were conducted in a single environment and did not attempt to distinguish pulled and pushed expansions; in part because there was no experimental population that could undergo both pulled and pushed expansions.

Experimental microbial populations are a tractable system to study ecological phenomena without the overwhelming complexity of the natural world. Yet, such experiments can guide our thinking, show which theoretical predictions may be observable in nature [45, 46], and help develop new models [47]. For example, range expansions of microbial populations have revealed the dependence of the invasion velocity on the supply of resources [48] and demographic stochasticity [44]. Experiments with microbes have also shown the strong effect of range expansion on competition [49, 50, 51, 52, 53, 54, 55] and neutral evolution via the founder effect or gene surfing [56, 57]. In this study, we focus on expansions with and without the Allee effect and quantify their differences. Since it is possible to control and measure population sizes in microbial populations over a few orders of magnitude, our experimental system is particularly well suited for studying the shape of the expansion fronts, as well as for future investigations on the rates of diversity loss and effects of habitat fragmentation such as invasion pinning [58, 14].

To recreate a range expansion in the laboratory, we used a metapopulation of budding yeast *S. cerevisae.* Yeast grows best at low densities on simple sugars such as glucose or galactose, but has a well-characterized Allee effect in the disaccharide sucrose [59, 13, 60, 61]. Sucrose is digested cooperatively because the yeast cells secrete an enzyme to hydrolyze extracellular sucrose into glucose and fructose, which are then transported into the cell. Higher cell densities facilitate the utilization of glucose, and therefore the growth rate of yeast on sucrose is maximum at intermediate population densities, where glucose utilization is high but competition is not strong enough. Importantly, the strength of the Allee effect can be controlled by tuning the relative concentrations of glucose and sucrose in the growth medium. Using this experimental system, we tested nontrivial properties of invasions including the exponential decay of population density at the front. We then observed the transition from pulled to pushed expansion waves as the Allee effect was made more severe, and found signatures of this transition in the expansion velocity and front shape. Our work confirms that Allee effects substantially affect invasion dynamics and demonstrates that pushed and pulled invasions can be distinguished by quantitative measurements.

2.3 Results

2.3.1 Experimental system

To study range expansions, we allowed the yeast populations to expand in one dimension along the columns of a 96-well plate. Each well represented a patch of suitable environment in a metapopulation where growth and death cycles occurred via a resupply of nutrients and dilution. Dispersal was achieved via exchange of small volumes of the growth media, corresponding to the migration rate (m), between the nearest wells (Fig. 2-1a). The experiments were started with a steep exponential initial population density profile, and after the profiles equilibrated over a few cycles, we used flow cytometry to measure the density profiles of the emergent waves. This allowed us to measure with high accuracy the velocity (v) and the spatial decay rate of the exponential front (λ) over multiple orders of magnitude of population density (Fig. 2-1b,c).

Range expansions of yeast in our metapopulations are well-described by the following model, which describes migration between nearest neighbor wells followed by growth over one experimental cycle:

$$n_{t+\Delta t,x} = g_{\Delta t}\left(n_{t,x} + D_{eff}\frac{\Delta t}{\Delta x^2}\left(n_{t,x+\Delta x} + n_{t,x-\Delta x} - 2n_{t,x}\right)\right) \tag{2.1}$$

Here, t and x are time and position; Δt and Δx are time of the dilution cycles and separation between the wells and is the dispersal rate determined by how much fluid is exchanged between the wells; D_{eff} is the dispersal rate determined by how much fluid is exchanged between the wells (see eqn. A.12 for the relationship between D_{eff} and the experimental parameter,m); and $g_{\Delta t}(n)$ specifies net growth during one cycle. Note that, in the limit of small Δt and Δx, this discrete model is equivalent to the well-known equation proposed by Fisher, Kolmogorov, and Skellam to describe biological invasions:

$$\frac{\partial n}{\partial t} = D\frac{\partial^2 n}{\partial x^2} + nr(n) \tag{2.2}$$

Thus our experiments can be viewed as both mimicking metapopulation dynamics typical for many ecosystems and approximating the continuous dynamics frequently assumed in mathematical ecology. The dynamics of pulled expansions are completely determined by linearized growth $\left(g_{\Delta t}(n_{t,x}) \approx n_{t,x}e^{r_0 \Delta t};\ r_0 = r(n=0)\right)$ and the expansion velocity is given by:

$$v_{lin} = min_{\lambda>0}\left(\frac{1}{\lambda \Delta t} ln\left[e^{r_0 \Delta t}\left[1 + \frac{D_{eff}\Delta t}{\Delta x^2}\left(cosh\left(\lambda \Delta x\right) - 1\right)\right]\right]\right) \approx 2\sqrt{r_0 D} \tag{2.3}$$

where the population density at the front decays exponentially with a rate λ, such that the velocity is minimized (eqn. A.10). In the limit of vanishing Δt and Δx, this gives the classic Fisher velocity, $v = 2\sqrt{r_0 D_{eff}}$, and the spatial decay rate of the population density at the expansion edge, $\lambda = \sqrt{r_0/D_{eff}}$.

In sharp contrast, the knowledge of linearized growth is not sufficient to determine the velocity of a pushed expansion, because immigration from fast growing regions behind the front increases the rate of invasion. Therefore, the deviations between the velocity and decay rate observed in the experiment and the corresponding values given by equation indicate that the expansion is pushed, not pulled. In our analysis, we use this difference between the observed expansion velocity and the linearized-growth-velocity to distinguish pulled and pushed waves.

2.3.2 Testing the theory of pulled waves

A surprising prediction for pulled waves is that the emergent properties of the wave front, its velocity (v) and spatial decay rate (λ), depend on the per capita growth rate of the population only at low density, r_0, and not at higher densities. To the first order, $v \propto \sqrt{r_0}$, and consequently, an apparently healthy population that grows to a very high carrying capacity can in fact be a poor invader if it grows slowly, as compared to a fast growing population that saturates at lower densities. To test this hypothesis, we compared the range expansion of *S. cerevisae* in two different media: 0.125% glucose, and 0.5% galactose. In both media, growth was exponential at low densities (Fig. 2-2a), but the two carbon sources showed a trade-off between faster low-density growth versus higher carrying capacity. Specifically, yeast cells initially grew at a faster rate in glucose, but saturated to a lower carrying capacity compared to galactose (Fig. 2-2b). Furthermore, there wasn't a measurable Allee effect in either media (Fig. A-2), and so we expected the expansions in both media to be pulled, and hence dependent only on the low-density growth rate. Consistent with the pulled-wave prediction, the resulting expansion waves indeed had a higher velocity in glucose, even though the bulk grew to a larger density in galactose (Fig. 2-2c).

To further quantify the qualitative agreement with theory that we observed above, we repeated the range expansion experiment in a wide range of environmental conditions, with the same two media, 0.125% glucose or 0.5% galactose. We varied the migration rate ($m = 0.4, m = 0.5$) and the death rate (diluting each cycle by amounts ranging from 2 to 4), which resulted in invasion velocities ranging from 0.2 *wells/cycle* up to 0.9 *wells/cycle*. Because the growth rate at very low densities needs to be known accurately, flow cytometry was used to count the number of divisions (fold growth) that cells undergo over the course of each 4 hour cycle (Fig. A-2). We found excellent agreement between the experimentally observed velocities and the linearized-growth-velocities predicted based only on the rates of dispersal and growth at low densities (Fig. 2-3a). Although this agreement is expected given the near-logistic growth in glucose and galactose, it provides a quantitative confirmation of the theory of pulled waves.

A similar comparison between the observed and predicted spatial decay rates was more challenging due to stochastic effects and long equilibration times. Stochastic effects appear due to the small number of individuals at the front and create much larger deviations between the deterministic theory (Eqn. 2.1) and the actual population dynamics for the spatial decay rate compared to the velocity (Fig. A-4). These deviations are known to make the fronts steeper (larger λ) [62, 63]. Instead of using the analytical approximations that account for the stochastic effects, we chose a more direct and precise approach to test the theory of pulled waves. Since the distinction between pulled and pushed waves lies only in the degree to which the growth dynamics can be linearized, we performed individual-based simulations that included demographic fluctuations using only the growth rate measured at low densities. For pulled but not pushed waves, the observed velocity and spatial decay rates must match simulations. As expected for expansions in glucose and galactose environments, the observed spatial decay rate was generally close to simulated values confirming that these expansions are pulled (Fig. 2-3b). However, moderate deviations were observed under some experimental conditions. All four of these outliers occurred when the predicted spatial exponent was much smaller than that of the initial profile. As a result, these expansion profiles required much longer time to reach their equilibrium shape and could still be out of equilibrium by the end of our experiments. Thus, the observed deviations might be due to insufficient observation time rather than the deviations from the theory of pulled waves.

2.3.3 Expansions transition from pulled to pushed as cooperativity increases

Populations in which the per capita growth rate decreases monotonically with increasing density always expand as pulled waves [64]; similarly, expansions of populations with a strong Allee effect are always pushed [29]. However, populations with a weak Allee effect may be either pulled or pushed, depending on the magnitude of the Allee effect (Fig. 2-4a). Thus, the transition from pulled to pushed waves occurs at some intermediate magnitude of the Allee effect, within the weak Allee effect regime (Fig. 2-4b).

To study this transition from pulled to pushed waves with increasing magnitude of the Allee effect, we studied the expansion of yeast on sucrose, where growth is known to be cooperative. In our experiments, low-density growth rate measurements in 2% sucrose showed an Allee effect over densities ranging from $\sim$ 103 to 105 *cells/well*, where the per capita growth rate increased with density (Fig. 2-5a). We note that this region of inverse density dependence is two orders of magnitude below the carrying capacity. As a result, the Allee effect would not have been visible with optical density measurements alone, and it was only revealed by fold growth measurements using flow cytometry - a situation that parallels the difficulty of detecting Allee effects in natural populations. We show below that even this weak Allee effect was sufficient to make the expansion in 2% sucrose pushed instead of pulled.

We tuned the magnitude of the Allee effect by modulating the amount of sucrose in the media. As sucrose concentration is increased, the growth rate at very low densities increases slowly, because only a fraction of the hydrolysis products can be captured before they diffuse away (Fig. A-7). In contrast, the maximal per capita growth rate, observed at intermediate cell densities, increases much more rapidly because dense populations use sucrose more efficiently (Fig. A-5). As a result, the magnitude of the Allee effect, measured as the difference between the low-density and the maximal per capita growth rate, increases with increasing sucrose concentration (Fig. A-8). Thus, by looking at expansions in different concentrations of sucrose, we were able to observe the transition from pulled to pushed expansions. We found that up to a sucrose concentration of 0.07%, the observed velocities were close to the linearized-growth-velocities, indicating that the expansions were pulled. However, as the Allee effect increased in magnitude, the observed and linearized-growth-velocities started to differ, reflecting the transition to pushed expansions (Fig. 2-5b).

We further confirmed that the observed differences between the pushed and the pulled waves were significant, by focusing on three sucrose concentrations: 0.22%, 0.67% and 2%. Since the migration rates were known and the low-density growth rates were measured, we could directly compute the linearized-growth-velocity in each of the environments and compare it to the experimentally measured rate of invasion. While the velocities of pulled waves fluctuated in a small region around the linearized-growth-velocities due to demographic and environmental stochasticity, the expansion velocities at high sucrose concentrations were much larger than, and well separated from, the corresponding linearized-growth-velocities (Fig. 2-5c). Thus, we indeed observed a transition from pulled to pushed waves.

We also tested whether the transition from pulled to pushed waves occur in our simulations when we use the entire dependence of the growth rate on population density. For high sucrose concentration we found that the expansion velocity in simulations with the entire growth curve exceeded the linearized-growth-velocity. However, the simulated and experimentally observed expansion velocities differed quantitatively, possibly because of the insufficient number of measurements of the growth rate at high cell concentrations (Fig. A-6).

To illustrate the difference between pulled and pushed waves, we compared a pulled expansion in glucose to a pushed expansion in sucrose with the same velocity and dispersal rate. If both waves are pulled, the density profiles must have identical decay rates, but, if the expansion in sucrose is pushed, then it must have a steeper front. Keeping all other experimental parameters the same, media with 0.125% glucose allowed such a comparison. The low-density growth rate in 0.125% glucose was marginally higher than in 2% sucrose (Fig. 2-5a), and the velocity of expansion in both the glucose and sucrose environments was nearly the same within measurement error. However, the spatial decay rates of the wave fronts were very different for the two waves. As predicted, the wave profile in sucrose was steeper than that in glucose, providing additional support to our finding that expansion in sucrose was a pushed wave (Fig. 2-5d) and demonstrating that the differences in the decay rates can also be used for distinguishing pushed from pulled expansions.

2.4 Discussion

Although range expansions have been studied extensively in ecology, many theoretical predictions have remained untested. Since pulled and pushed waves appear qualitatively similar, with a constant expansion velocity and exponential fronts, expansions are often assumed to obey the universal theory of pulled waves. Our study provides a proof of principle that pulled and pushed waves can be distinguished with quantitative measurements. We demonstrated that these two classes of expansions can be empirically distinguished based on the violation of the expected relationship between the velocity and either the front shape or the low-density growth rate. At the same time, our work also shows that such measurements are difficult even in the controlled laboratory settings.

Distinguishing between pushed and pulled expansions could be important for forecasting invasion dynamics and understanding species evolution. Predicting the rate of colonization may be particularly challenging for pushed waves because they can advance slowly in the beginning due to an Allee effect, but accelerate later as the bulk density increases [58, 6]. Pushed waves are also expected to have slower rates of neutral evolution and diversity loss compared to pulled expansions [37, 65]. The conservation strategies to limit pulled and pushed invasions could also be very different. For pulled waves, the best way to limit the expansion is to eradicate the invaders at the very edge of the expansion. In contrast, a balanced eradication strategy over the entire invasion front is more effective for pushed waves [58, 66].

Beyond the specific results described above, our work established a tractable experimental system where many ecological and evolutionary scenarios or theories can be tested. Given the increasing rate of range shifts, it is important to experiment with how populations respond to unavoidable changes in their spatial distribution as well as to specific ecological perturbations designed as mitigation measures. Laboratory microbial systems could be very useful for studying such phenomena in greater detail, complementing more realistic but less tractable field studies.

Some questions that can be immediately investigated in our experimental system are the response of invasions to environmental fragmentation and the effects of range expansions on species evolution. Habitat fragmentation is likely to increase due to anthropogenic activities and might be especially important for species moving to barely hospitable regions as they escape the warming climate. Theory predicts that pushed, but not pulled, waves can become pinned or stuck in a fragmented environment, yet empirical tests of this prediction are scarce. Species evolution also depends critically on whether it invades as pulled or a pushed wave. For example, the founder effect has a much greater role in pulled compared to pushed invasions. Quantitatively experiments in controlled laboratory settings are likely to provide valuable insights into these important phenomena.

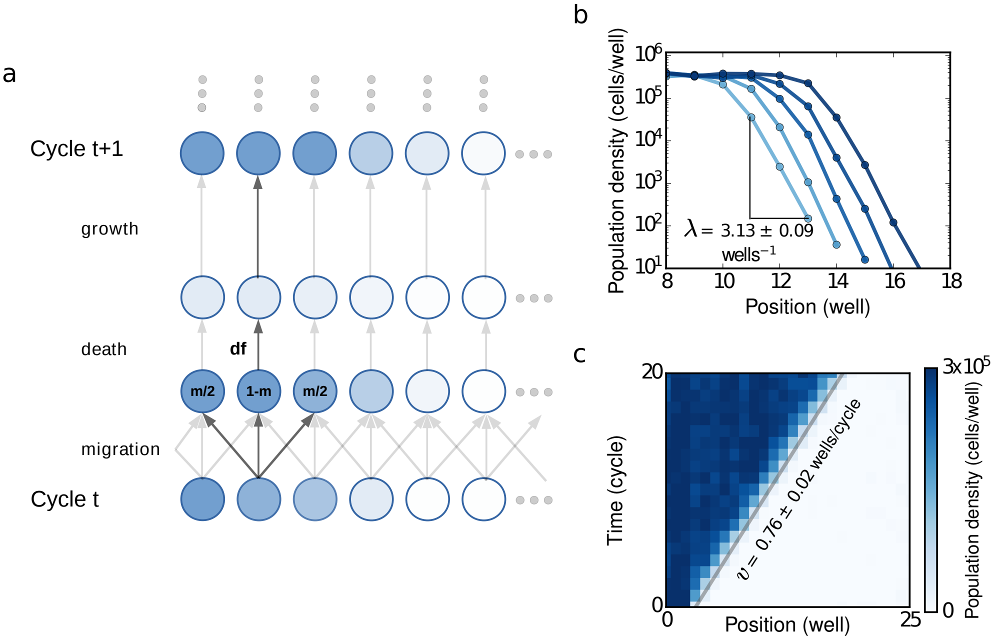

Figure 2-1: **Theoretical predictions for the velocity and spatial density profile of pulled and pushed waves were quantitatively tested in metapopulations of budding yeast, *S. cerevisae*, in a controlled experimental setup.** (a) Yeast populations expanded along the columns of a 96-well plate. The experiments were started with an exponentially decaying spatial density profile. After every growth cycle of 4 hours, cells were diluted into a new plate and dispersal was achieved by transferring small amounts of media to neighboring wells along the columns (b) Optical density measurements at the end of each cycle revealed an emergent wave traveling at constant velocity. (c) At later times, after allowing the fronts to equilibrate, the density profiles were also measured using flow cytometry. These high resolution measurements at the low density fronts showed exponential fronts extending over 4 orders of magnitude in density. The spatial decay rate (SDR), λ, was estimated by averaging over density profiles over the last few cycles, after the expansion wave had equilibrated. The profiles measured using flow cytometry were also used to measure the velocity more accurately (SI A.1).

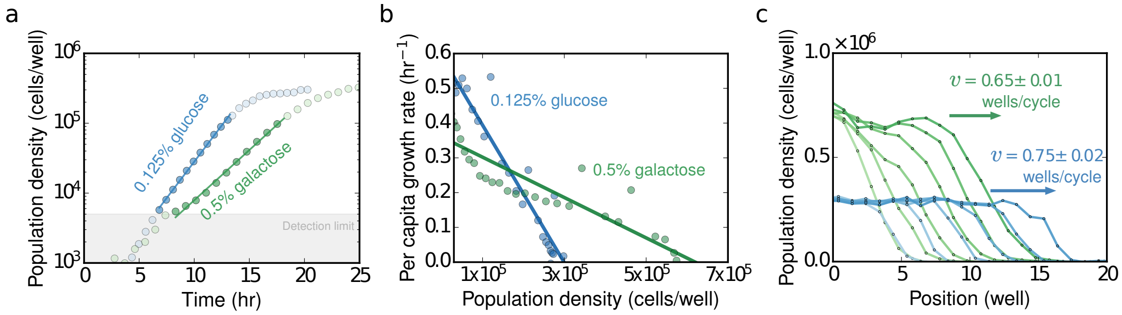

Figure 2-2: **In pulled waves, expansion velocity depends on the growth rate only at low densities irrespective of the carrying capacity.** (a) A population of *S. cerevisiae* grows exponentially at low densities in 0.125% glucose and 0.5% galactose. Growth rate at low densities is higher on 0.125% glucose compared to 0.5% galactose, and decreases monotonically in both environments. (b) The galactose environment has a higher carrying capacity compared to glucose. The two environments thus show a trade-off between the low-density growth rate and the carrying capacity. (c) Although the galactose environment is more favorable in terms of the total nutrient availability (carrying capacity), expansions are faster in glucose because the populations grow faster in glucose at low density.

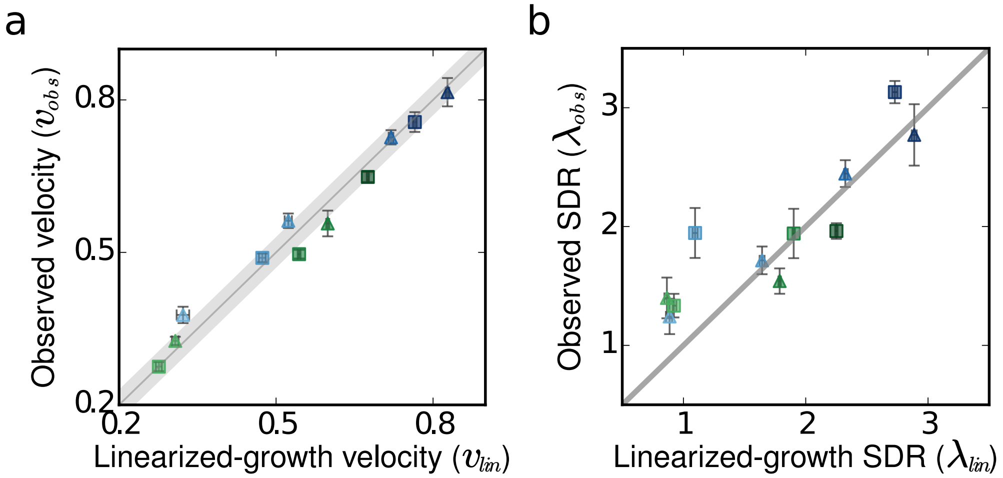

Figure 2-3: **For pulled waves, the growth rate at low density is sufficient to determine the emergent wave properties quantitatively. Over a wide range of environmental conditions, the observed expansion velocities and the spatial decay rates (SDR) of the population density at the front closely match the predictions based on the measured low-density growth rate.** (a) Predicted and observed velocities in two different media are shown (glucose in blue, galactose in green). The migration rate (triangles: $m = 0.5$, squares: $m = 0.4$) and the death rate (darker colors are smaller death rates) were varied. Independently measured growth rates, only at low densities, in the two different media were sufficient to predict the velocities accurately. (b) A similar comparison for the spatial decay rates (λ, $well^{-1}$) also shows close agreement for steep predicted fronts (large λ). However, shallow predicted fronts deviated slightly from predictions, which may be a consequence of the long relaxation time to equilibrium for such fronts. x-axis error bars: standard error of the mean of the measured low-density growth rates, propagated to the errors in predicted velocity (a) and spatial decay rate (b). y-axis error bars: (a) standard deviation of velocity measured for five different thresholds, and (b) standard deviation in spatial decay rate measured over three different regions of the front.

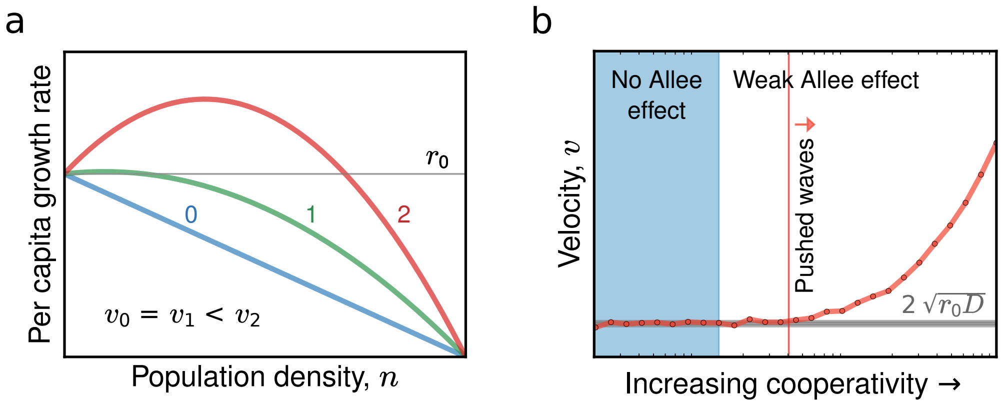

Figure 2-4: **Expansions transition from pulled to pushed at an intermediate strength of Allee effect within the weak regime.** (a) Three different growth profiles displaying with increasing magnitude of Allee effect (growth profile 0 is purely logistic; 1, 2 have a weak Allee effect), but with the same low-density growth rate. Unlike pulled waves, the velocities of expansion in the three cases are not the same. In particular, both logistic (0) and the less severe Allee effect (1) result in pulled waves with the same velocity, given by $2\sqrt{r_0 D}$. In contrast, condition (2), with a larger but still weak Allee effect leads to a pushed wave with velocity greater than $2\sqrt{r_0 D}$. (b) To illustrate the transition from pulled to pushed waves in the weak Allee effect regime, we simulated expansions using a model (eqn. A.13), keeping growth rate at low density constant at r_0. The velocities begin to deviate from predictions based on the low-density growth rate, once cooperative effects start to contribute significantly to growth. When growth rate decreases monotonically (blue shaded region), the resultant expansions are always pulled. For low cooperativity (up to the red line), the expansions are pulled, even though there is a weak Allee effect. Beyond the threshold, however, the expansions are pushed, reflected in the deviations from the linearized-growth-velocities.

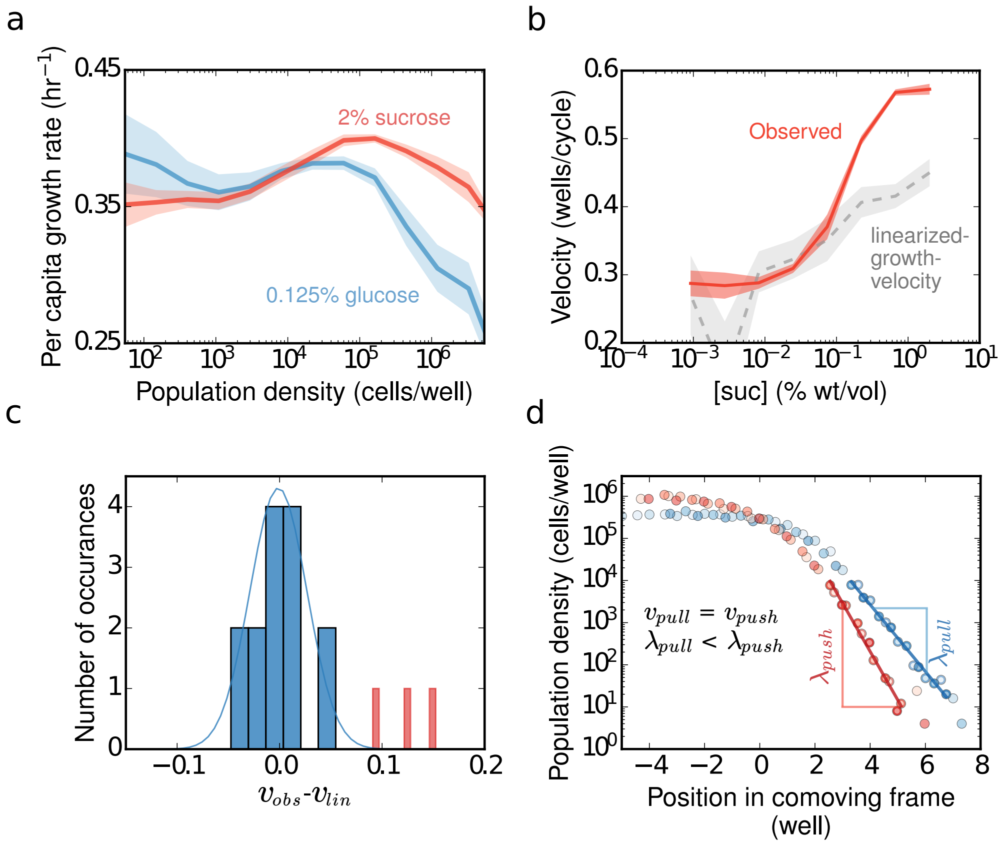
a
Per capita growth rate (hr^{-1})
0.45
0.35
0.25
2% sucrose
0.125% glucose
10^2 10^3 10^4 10^5 10^6
Population density (cells/well)
b
Velocity (wells/cycle)
0.6
0.5
0.4
0.3
0.2
Observed
linearized-growth-velocity
10^{-4} 10^{-3} 10^{-2} 10^{-1} 10^0 10^1
[suc] (% wt/vol)
c
Number of occurances
0 1 2 3 4
−0.1 0.0 0.1 0.2
v_{obs}-v_{lin}
d
Population density (cells/well)
10^0 10^1 10^2 10^3 10^4 10^5 10^6
$v_{pull} = v_{push}$
$\lambda_{pull} < \lambda_{push}$
λ_{push}
λ_{pull}
−4 −2 0 2 4 6 8
Position in comoving frame (well)

Figure 2-5: **A sufficiently large Allee effect gives rise to pushed waves that can be identified based on their deviations from predictions based on linearized growth.** (a) Experimental measurement of growth rates in sucrose (red) and glucose (blue) show that growth rate in glucose decreases monotonically with increasing density. In sucrose, the per capita growth rate increases with density for densities ranging from 10^3 to 10^5 *cells/well*. This weak Allee effect is sufficient to cause the expansions in sucrose to be pushed. (b) The prediction that increasing magnitude of Allee effect leads to a transition from pulled to pushed waves was tested by increasing the sucrose concentration in the media, which increases the magnitude of the Allee effect (Fig. A-8). Confirming our expectation, the observed velocities deviated significantly from pulled-wave predictions (linearized-growth-velocities) for high sucrose concentrations, indicating a transition into the . Under all of these conditions, the Allee effect was weak. Shaded region indicates S.D. in measured velocity (red) and S.E.M. of low-density growth rate propagated to the error in predicted velocity (gray). (c) Pushed waves can be quantitatively distinguished from pulled waves based on the deviations of observed velocity from linearized-growth predictions. Although the observed velocities of pulled waves were distributed around the predicted velocities (based on linearized growth), observed velocities of pushed waves were well separated from this distribution and clearly distinguishable (p-value 0.0015). (d) Superimposing the front profiles at different times after equilibration (which is the same as observing the wave profile in a frame moving with the same velocity as the front - the comoving frame), allows for a more accurate measurement of the spatial decay rate of the front. Measurements in this comoving frame show that when conditions are chosen so that the glucose and sucrose waves travel at the same velocity, the pushed wave in sucrose is steeper than the pulled wave in glucose. Thus, pushed waves can be distinguished from pulled waves based on their deviation from the universal relationship between either the low density growth rate and velocity, or velocity and front shape.

Chapter 3

Cooperation mitigates diversity loss during microbial range expansions

3.1 Significance statement

Spatially expanding populations lose genetic diversity rapidly because of the repeated bottlenecks formed at the front as a result of the serial founder effect. However, the rate of diversity loss depends on the specifics of the expanding population, such as its growth and dispersal dynamics. We have previously demonstrated that changing the amount of within-species cooperation leads to a qualitative transition in the nature of expansion from pulled (driven by migration at the low density tip) to pushed (driven by migration from the high density region at the front, but behind the tip). Here we demonstrate experimentally that pushed waves, caused in the presence of sufficiently strong cooperation, result in strongly reduced genetic drift during range expansions, thus preserving genetic diversity in the newly colonized region.

3.2 Introduction

Spatial population expansions occur at multiple scales, from the growth of bacterial biofilms and tumors to the spread of epidemics across the globe [67, 68, 69]. Natural populations often undergo range shifts or range expansions, in response to changing climate [20, 70], and increasingly, following introduction into novel geographical areas due to trade, travel and other anthropogenic factors [7]. The fate of moving populations depends on their genetic diversity, which allows them to adapt to the new environment [71]. The very process of spatial expansion is, however, predicted to erode the diversity of the population [72, 73], since the newly colonized territory is seeded by only a subset of the genotypes that exist in the original population. This phenomenon, known as the founder effect, greatly amplifies genetic drift in the population and leads to diversity loss and accumulation of deleterious mutations [74, 75, 12]. Thus, a firm understanding of the founder effect is necessary to predict and control the fate of expanding species.

While diversity is lost during all expansions, the rate of loss is expected to be strongly influenced by the expansion dynamics, which depend on the details of dispersal and growth. Expansions can be classified into two categories - pulled and pushed [76, 29]. In populations that do not exhibit any within-species cooperation, the growth rate is maximum at low densities and decreases monotonically as the density increases. In such populations, migrants at the low density tip of the wave grow at the fastest rate, and drive the expansion into the new area. Such expansions are called pulled waves, and their expansion velocity, also known as the Fisher velocity, depends solely on the diffusion rate of the individuals and the growth rate of the species at low density. On the other hand, pushed waves occur in the presence of cooperative growth within the population (i.e. positive density dependence of the growth rate, also known as the Allee effect) whereby the tip grows at a much lower rate than the higher density bulk [77, 31]. Since the growth rate at low density in such populations is lower than in the bulk, the fisher velocity for such populations is lower than the actual expansion velocity. The difference in the dynamics of pulled and pushed waves has substantial genetic consequences [56, 78, 79, 80, 65, 81].

In its simplest form, range expansions can be viewed as a series of founding events, where a small subsample of a population establishes a founding colony in a new territory and then grows rapidly even as the process repeats itself. The series of population bottlenecks at each of the founding events quickly erodes the genetic diversity in the population, in a process aptly called the serial founder effect. However, among species with the Allee effect, growth in the low density founding colonies is much more subdued, and the colonization of the new territory is driven by migrants from well-established high-density regions with high genetic diversity, rather than by the quick growth of the founders. Consequently, populations experiencing the Allee effect are predicted to maintain genetic diversity over longer distances and times (Fig. 3-1A).

This differential rate of diversity loss in pulled and pushed waves is well-characterized in a wide range of theoretical models [56, 78, 79, 80, 65, 81, 37, 82, 83], and has also been observed empirically in field studies [10, 84, 38]. However, it has been difficult to directly connect the empirical observations to theory [10], in part because these natural expansions cannot be replicated, and also because numerous environmental factors cannot be as well-controlled. Microcosm experiments have helped address this chasm between theory and experiments by partially trading off realism for much better controlled and replicable biological systems [85, 42, 86, 87]. Indeed, some ingenious experiments with bacterial colonies expanding on agar have previously demonstrated diversity eroding and diversity preserving range expansions [46, 56, 49, 53]. In these experiments, microbial colonies expanded on the surface of agar, and formed monoclonal sectors during expansion, leading to loss of diversity. However, this sectoring phenomenon was lost when two different mutualist species were inoculated together at the center instead of a single species. The sector formation in the former case and its lack in the mutualists can be well-understood mechanistically for this particular system in terms of the (microscopic) demographic and geometrical properties of the expanding species. In contrast, in our current study, we explore the differential rate of diversity loss more generally as a consequence of growth demographics, independent of species-specific mechanisms.

We endeavor to experimentally understand the genetic consequences of range expansions using the framework of pulled and pushed waves with a focus on establishing the general relationship between cooperatively vs competitively growing populations, and their neutral evolution during expansion. Towards this end, we extend a previously developed experiment, where we demonstrated the transition from pulled to pushed waves with increasing cooperation in yeast [16], to now include two otherwise identical genotypes with different fluorescent markers, whose frequency can be tracked to study neutral evolution. We find that yeast populations expanding as a pulled wave undergo a drastic reduction in genetic diversity, unlike the same population expanding as a pushed wave. Moreover, we quantify the rate of diversity loss in terms of the effective population size, and show that the effective population size correlates well with how pushed the expansion is (aka 'pushedness').

We also observe a few evolutionary jackpot events during which one of the genotypes abruptly increases in frequency. Such events are predicted to arise naturally due to rare stochastic excursions of the expansion front ahead of its expected position [88]. Our results support this theory because abrupt changes in allele frequency co-occur with substantial changes in front shape. Importantly, we show that these evolutionary jackpot events can be distinguished from selective sweeps without additional follow up experiments.

3.3 Results

The stepping-stone metapopulation model is widely used to describe the spatiotemporal population dynamics in patchy landscapes [28]. In this model, populations grow in discrete patches that are connected to nearest neighbor patches via migration, which is reflected in our experimental setup. The budding yeast, *S. cerevisiae*, expands in one dimension, along the rows of a 96-well plate, with cycles of growth, nearest-neighbor migration, and dilution into fresh media (Fig. 3-1B). At the beginning of every cycle, a fixed fraction ($m/2$) of culture in each well is transferred into wells at adjacent locations on either side, while the remaining ($1 - m$) is transferred into the well at the same location (migration rate, $m = 0.4$, unless stated otherwise). At the same time, the culture is also diluted into fresh media by a constant factor. After dilution, the cultures are allowed to grow for 4 hours before the cycle is repeated. Starting with a steep initial spatial density profile of yeast, this process leads to a stable wavefront (as defined in Fig. 3-1A, Materials and Methods (B.1)) moving at a constant velocity (Fig. 3-2A).

Previous studies have shown that yeast typically do not display cooperative behavior when growing on simple sugars such as galactose or glucose, but grow cooperatively on sucrose [59]. Thus, without any Allee effect, we expect that expansions in galactose and glucose would lead to pulled waves, where the velocity is given by the Fisher velocity. We confirm this in experiments, by first explicitly measuring the low-density growth rate of our strain (DH, Materials and Methods (B.1)) in galactose (Fig. B-1). We also measure the expansion velocity and spatial density profile using flow cytometry, and find that it is indeed consistent with the Fisher velocity corresponding to the measured growth rate. We thus establish that the expansions in galactose are pulled waves.

3.3.1 Loss of diversity during expansions

In order to quantify the neutral genetic drift during these pulled expansions, we use two otherwise identical genotypes of the same strain, but with different constitutively expressed fluorescent markers, whose frequency can be tracked using flow cytometry. We start with a 1:1 ratio of the two strains in the initial density profile for the expansion experiment. Over the course of about 100 cycles, the relative frequencies of the two genotypes in the expansion front (as defined in Materials and Methods) change rapidly, undergoing large fluctuations, occasionally leading to fixation of one of the genotypes. Tracking the genotype fractions over 24 replicate realizations of the experiment reveals that while the waves are nearly identical in terms of the velocity and wavefront shape, the internal dynamics of individual fractions is highly different (Fig. 3-2B). This can be clearly seen from the variance in fractions across replicates (Fig. 3-2E), which grows from 0 at the beginning of the experiment to the maximal value of 0.5. The measured variance allows us to quantify the rate of loss of diversity in terms of the effective population size using the following relationship:

$$var(t) = f_0(1 - f_0)\left(1 - exp\left(\frac{-t}{N_{eff}}\right)\right) \tag{3.1}$$

where $var(t)$ is the variance in the fractions across replicates as a function of time, $f_0 = 0.5$ is the initial fraction at $t = 0$, and t is in the units of generation time (cycles in this case, since the entire front is effectively diluted by 2x every cycle, and so, each cycle corresponds to one generation). For the pulled waves in galactose, the effective population size is approximately 210 - four orders of magnitude smaller than the actual size of the population in the wavefront (Fig. 3-2E). We thus see that there is a tremendous loss of genetic diversity during pulled expansions.

We repeat the same experiment, but now with yeast growing on sucrose, where we expect growth to be cooperative and hence, the expansions to be pushed [16]. The expansion speed and bulk population density in sucrose is similar to that in galactose (Fig. 3-2A). Yet, while the waves are physically similar, their effect on the genetic diversity is drastically different. The frequencies of the two genotypes, starting at an equal 1:1 ratio, remain almost unchanged at the end of the experiment (Fig. 3-2D). The diversity preserving nature of these pushed expansions is reflected in the large effective population size, estimated to be higher than 15,000 - at least two orders of magnitude larger than in pulled waves (Fig. 3-2E).

3.3.2 Effective population size is correlated to the 'pushedness' of expansion wave

While the dynamics of genotype fractions during galactose and sucrose expansions is consistent with intuition from theory, the dynamics of fractions during expansions in another simple sugar, glucose, are observed to be rather surprising. Although we expect the expansions to be pulled, and hence lose diversity quickly, similar to the galactose expansions, the effective population size in glucose is actually intermediate between that in galactose and sucrose (Fig. 3-2C,E). Diversity during glucose expansions is lost much faster than in sucrose, but not quite as rapidly as in galactose.

In order to better understand the unexpected behavior in glucose, we explicitly test the pulled or pushed nature of expansions in all three media. Pulled waves expand at the Fisher velocity, which is determined solely by growth rate at low density and the migration rate, while pushed waves expand at a velocity greater than the Fisher velocity. We define a 'pushedness' parameter, given by the ratio of the actual velocity to the Fisher velocity, so that pushedness $= 1$ for pulled waves, and > 1 for pushed waves. Indeed, the pushedness of the galactose expansions is observed to be close to 1, whereas that for sucrose is 2.3, clearly confirming that the galactose expansions are pulled and the sucrose ones are pushed (Fig. 3-3A). Surprisingly, the pushedness for glucose expansions is also greater than 1, suggesting that contrary to our naïve expectation, the waves in glucose are in fact not pulled. More careful measurements of the growth profile of the DH strains in 0.2% glucose reveal a very tiny amount of cooperative growth at extremely low densities (below $10^3 cells/well$), making them very weakly pushed (Fig. B-1). While this Allee effect might originate due to many possible factors such as collective pH modulation [89], it is important to note that the emergent property of the wave, pushedness, explains the decreased rate of diversity loss without the need to understand species-specific growth mechanisms.

We further probe the relationship between pushedness and the rate of diversity loss experimentally, by repeating the expansion experiments in multiple environments using two different pairs of strains (DH-RFP/DH-CFP and BY-RFP/BY-YFP). The different strain-media combinations give rise to expansions spanning a broad range of pushedness values (Fig. 3-3B). We find that the pushedness correlates well with the effective population size during expansions (Fig. 3-3C). Broadly, for all instances of pulled waves, Neff was under 500, over four orders of magnitude below the actual population size. Within the pushed waves, we find two regimes with very different rates of diversity loss. In the weakly pushed regime, the effective population size ranged between 500 and 4000. We thus see that even for pushed waves, if the cooperativity is not strong enough, diversity can be lost quite rapidly. Finally, in thestrongly pushed regime, we can only set a lower bound on the effective population sizes (Materials and Methods), and the lower bounds are at or over 15,000 (Fig. 3-3C). Overall, for populations with approximately equal bulk densities within a factor of 3, the rate of diversity loss is seen to be strongly modulated by the pushedness.

3.3.3 Distinguishing selective sweeps from jackpots

Throughout our experiments, we observe a few instances where one of the genotypes appears to take over the population very rapidly. Fig. 3-4A shows two such rapid takeover events, which closely resemble evolutionary sweeps. However, during range expansions, such sweeps can also occur purely as a consequence of spurious migration. For instance, rare long distance dispersal might help establish a clonal population in an unoccupied territory near the front. This clonal population merges with the expanding front, resulting in a sudden increase of the fraction of that genotype in the front. This process, called the 'embolism effect' has been previously proposed in theoretical literature [83], and we found one instance of it in our experiments (Fig. B-2). In addition to embolism, rapid takeovers in experiments might also occur when a clump of cells of the single genotype is transferred over to the front of the wave, leading to increased frequency of that genotype in the front. As the expansion progresses, this increased frequency propagates to higher and higher densities till it takes over the entire front (Fig. 3-4B, top panel). We call this phenomenon a jackpot, to distinguish it from aa selective sweep, and observe it in simulations as well, in the presence of noisy migration (Fig. 3-4B,C).

The excess migration at the front that results in jackpots enables us to distinguish them from selective sweeps. As a consequence of the excess migration, the wavefront widens (i.e. the front width increases) transiently (Fig. 3-4B, bottom panel). This also leads to the wave expanding faster transiently, but both the velocity and front width return to their mean values as the front equilibrates back. We confirm this mechanism in simulations, where, by following the trajectory of a rapid takeover event in the front width - velocity state-space, we see the transient front widening accompanied by an increased velocity, before the trajectory returns to the mean front width and velocity (Fig. 3-4E). On the other hand, selective evolution towards a higher growth rate (migration rate is fixed in our assay and cannot be selected for) leads to increased velocity but decreased front width (front width of pulled waves

$\sim \frac{1}{\sqrt{r_0}}$, [29]). Moreover, in the case of selective sweeps, the trajectories in the velocity-front width space do not return to the previous mean, but rather settle at the new equilibrium. This phenomenological intuition is also confirmed by explicitly adding a low mutation rate in the simulations and following the state space trajectory during periods of rapid takeover (Fig. 3-4E).

Among the rapid takeovers that we observe in experiments, a subset can be clearly seen to follow the selection template. Fig. 3-4D shows the state space trajectory for one replicate that putatively evolved to a higher growth rate (red trajectory, compare to a jackpot shown in blue), corresponding to the takeover trajectories shown in Fig. 3-4A. We observe these putative selective sweeps only in a single growth medium among several that we used in our experiments; this medium was limiting in terms of an essential amino acid, and thus, is likely to apply a higher evolutionary pressure than the others. Taken together, this suggests that the rapid takeovers that we see in this particular medium are indeed instances of selective sweeps (Fig. B-3). We also observe a few rapid takeover events that do not follow the selection template, but rather, look like jackpots (Fig. B-2). In fact, even though the two fraction timeseries shown in Fig. 3-4A are nearly identical, the two can be clearly distinguished as selective sweep or jackpot based on their state space trajectories. Given the rarity of both jackpots and selective sweeps due to mutation, we only see anecdotal evidence of the two in our experiments. However, the few instances that we indeed see for both processes are consistent with theoretical predictions and simulations.

3.4 Discussion

In this study, we used a well-controlled laboratory microcosm setup to probe the distinct evolutionary consequences of pulled and pushed expansions. We observed the rapid loss of diversity due to the serial founder effect when yeast expanded as a pulled wave, and a much more subdued loss of diversity when it expanded as a pushed wave. Moreover, we found environmental conditions that span across different levels of pushedness, and saw that the effective population size in the front is strongly correlated with the amount of pushedness of the expansion wave. Thus, pushedness proves to be a useful measure in predicting the rate of diversity loss during range expansions. Finally, we also discovered that in one of the expansion media, the yeast evolved to have a higher growth rate, and we were able to distinguish such evolutionary sweeps from rapid takeovers occurring simply due to stochasticity, although they look very similar when only the genetic structure is being tracked.

The extensive theoretical work on range expansions has led to other very interesting predictions that could also be addressed using our experimental system. One prediction pertains to the quantitative dependence of the effective population size on the actual population size of the wavefront [82]. It has been established that, with growth and migration held fixed, N_{eff} scales linearly with N_{bulk} in fully-pushed expansions, and $N_{eff} \sim log^3 (N_{bulk})$ in pulled expansions. Moreover, in the presence of a very weak Allee effect, Birzu et al predict a third class of expansions that is intermediate between pulled and pushed, where N_{eff} scales sublinearly with N_{bulk}. We made an attempt to observe these different scaling relationships by varying the bulk population size in experiments in two different ways - by changing the total volume, and thus the population size, and by changing the amount of a limiting amino acid. Unfortunately, in the former case, the altered volume also altered the density-dependence of the growth, while in the latter case, the low amino acid condition led to evolution during expansion (Fig. B-1). We speculate that the expansions in glucose, where the loss of diversity is intermediate between galactose and sucrose, might in fact belong to the newly predicted third class of expansions. Modifying our assay to modulate the bulk density without changing growth properties would help resolve this speculation.

In addition to genetic drift, demographic stochasticity and environmental noise have also been predicted to cause fluctuations in the position of the expansion front [62, 88, 82], leading to its diffusion around the mean position. Much like the case of genetic drift, in pushed waves, the effects of demographic noise on front diffusion are predicted to be subdued, and the diffusion largely reflects environmental noise. In contrast, in pulled waves, front diffusion is predicted to be faster, owing to the large influence of demographic noise. We observefront diffusion in both pulled and pushed waves in our experiments, where the variance in front position remains constant for some initial period before it starts increasing linearly with time (Fig. B-4). However, we do not see a significant quantitative difference in front diffusion in pulled vs pushed waves, in part due to lack of a sufficiently long timeseries of data, and partly because environmental noise might be dominating both pulled and pushed waves.

Allee effects, or the inability of organisms to grow optimally at very low densities, is often considered to have a negative impact on populations. For instance, it leads to lower expansions velocities compared to the velocity if growth were not suppressed at the low density tip. However, in this study we demonstrate that the Allee effect can in fact have a very beneficial effect on the expanding population by helping preserve diversity as the population enters novel territories, where the diversity is especially critical for survival. Even a miniscule Allee effect at very low densities, such as we found in the glucose expansions, can go a long way in helping mitigate diversity loss. Perhaps such tiny Allee effects pervasive in many invading species explain the lower than predicted rates of diversity loss during their expansion.

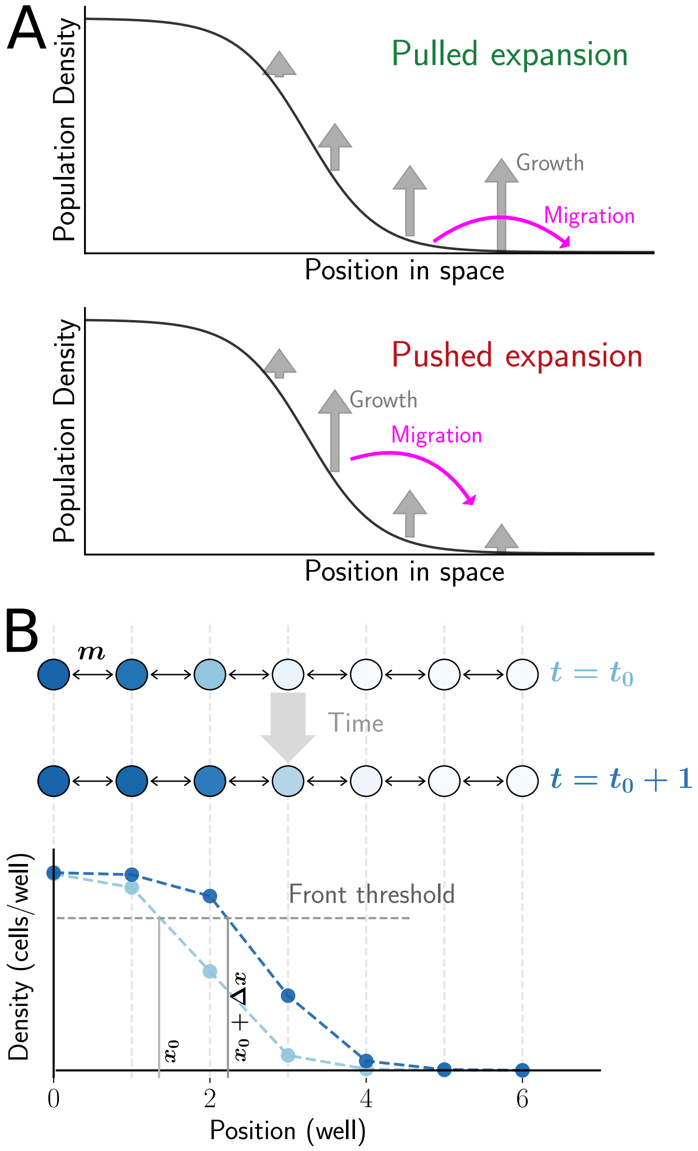
A
Population Density
Pulled expansion
Growth
Migration
Position in space
Population Density
Pushed expansion
Growth
Migration
Position in space
B
m
$t = t_0$
Time
$t = t_0 + 1$
Front threshold
Density (cells/well)
x_0
$x_0 + \Delta x$
0
2
4
6
Position (well)

Figure 3-1: **Yeast expanding in a 1D metapopulation landscape is used to study the genetic consequences of pulled and pushed range expansions.** **A.** Range expansions can be broadly classified as pulled or pushed depending on the primary drivers of the expansion. In pulled expansions, the small number of founders from the tip of the expansion grow rapidly in the new territory (top panel). This small founding population only contains a small subset of the total diversity in the bulk of the population. Thus, diversity is quickly eroded as the population expands into new area. Pushed waves are driven by migration out of the bulk, because the small density of founders at the front has a subdued growth rate (bottom panel). As a result, genetic diversity is maintained even as the population expands. **B.** The experimental setup consists of yeast expanding in a discrete space, discrete time 1D metapopulation landscape. Adjacent wells are connected via migration, and exchange a fixed fraction of cells, m, every cycle, and then grow for 4 hrs (top panel). This process results in an emergent wavefront of a fixed density profile moving to the right with a fixed velocity (bottom panel). The location of the wavefront is determined as the interpolated well position where the density profile crosses a predetermined threshold. Velocity is then measured as the rate of advance of the wavefront location. The entire area to the right of the threshold location is defined as the 'front' for subsequent computation of genotype frequencies.

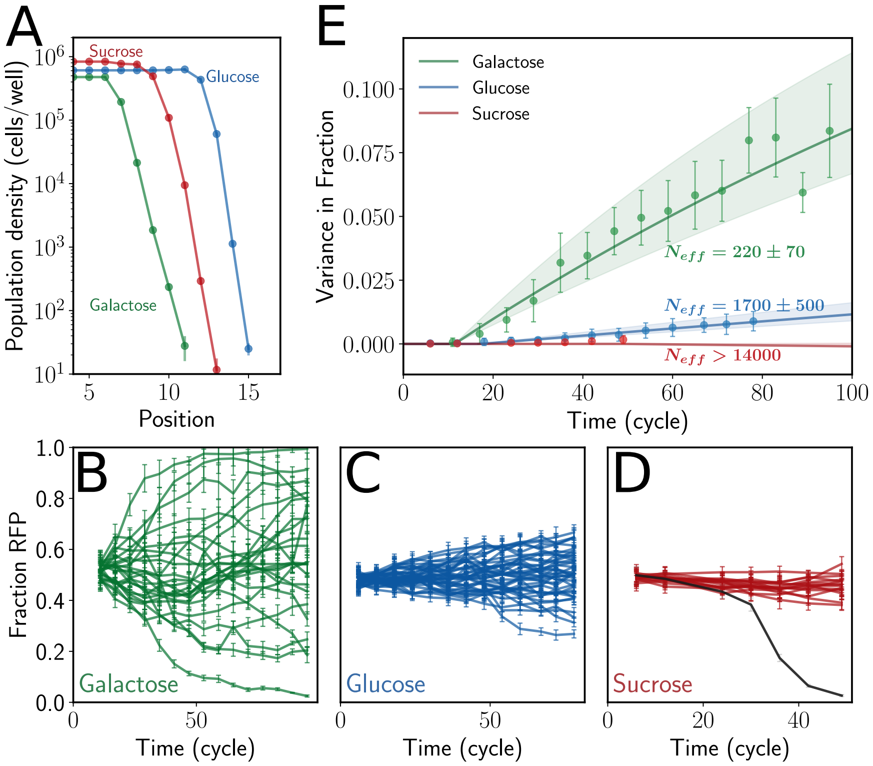

Figure 3-2: **Yeast expanding in different growth media loses diversity at very different rates even though the wavefronts have similar physical properties, such as velocity and bulk density A.** Populations of *S. cerevisiae* growing in galactose, glucose or sucrose media expand spatially in a 1-dimensional discrete landscape as traveling waves with a constant velocity and an exponentially decaying wavefront. The velocities, population density in the bulk as well as the spatial profile are similar in all three environments. **B.** Yeast expanding on galactose lose diversity drastically. Starting with equal initial frequencies of two genotypes that differ only in terms of a single fluorescent marker (RFP or CFP), the fraction of one of the genotypes in the front (RFP) fluctuates randomly, before reaching fixation on some occasions. The expansion experiments are replicated 24 times, and the dynamics of fractions varies by a large amount across replicates. **C, D.** The same experiments when repeated in different media, glucose and sucrose, show very different rates of diversity loss and fraction dynamics. In glucose (**C**), although we still see a loss of diversity over time, it is much slower compared to the galactose expansions. When expanding in sucrose (**D**), we do not see a significant loss of diversity over the observed time period (the replicate shown in grey was mis-pipeted in cycle 30, and hence diverges from the rest (SI). This replicate is ignored in further analysis). **E.** The rate of diversity loss can be quantified in terms of the rate of increase of variance in fractions across replicates as a function of time (Eqn. 2.1, $f = 0.5$). In galactose and glucose, the variance increases significantly above zero, allowing us to quantify the effective population size. In sucrose, the increase in variance is not statistically significant, allowing us to only set a lower bound on the effective population size. The drastic loss of diversity in galactose is reflected in the effective population size in the expanding front, ~ 220, over four orders of magnitude lower than the actual population size in the front. Effective size in glucose is around 1500, and that in sucrose is estimated to be over 15,000.

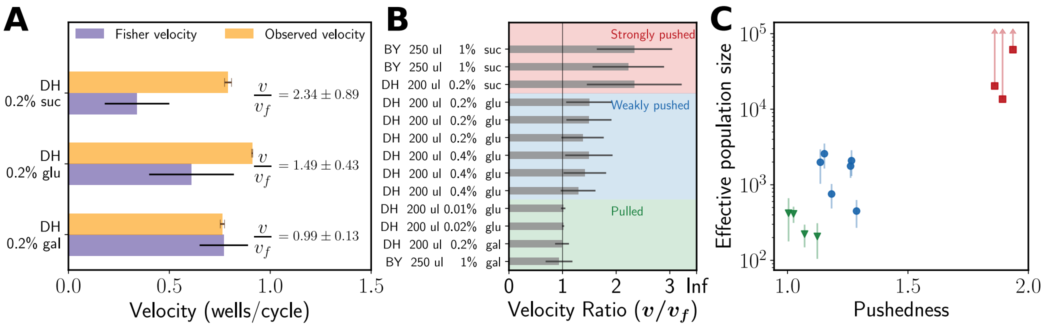

Figure 3-3: **The ratio of observed velocity to the Fisher velocity (defined as the pushedness) determines the rate of diversity loss during expansions** **A.** Range expansions can be pulled or pushed as defined in terms of the ratio of the observed velocity to the Fisher predicted velocity, which we define as the pushedness of the expansion. Pulled waves expand at the Fisher velocity, and have a pushedness of 1, whereas pushed waves have pushedness larger than 1. Consistent with the observed rates of diversity loss, the waves in galactose have pushedness $= 1$, and those in sucrose have pushedness $= 2.3$, much larger than 1. Surprisingly, expansions in glucose were also found to be pushed (even though, given that glucose is a simple sugar, we expect growth to not be cooperative in glucose), although not as strongly as those in sucrose. This explains the intermediate rate of diversity loss in glucose compared to galactose and sucrose. **B.** We repeat the expansion experiments across multiple environmental conditions (media, death rate, migration rate), for two different pairs of yeast strains (BY and DH) and observe a wide range of pushedness values for the different expansions. **C.** Effective population size is plotted against the pushedness for the different strain-media combinations. We find that N_{eff} correlates strongly with the pushedness. For pulled waves, the effective population size is between 100 to 700 - over 4 orders of magnitude lower than the actual population size in the wavefront. For pushed waves, the effective size is over 15,000, much closer to the actual size in the wavefront, which is of the order of 10^6.

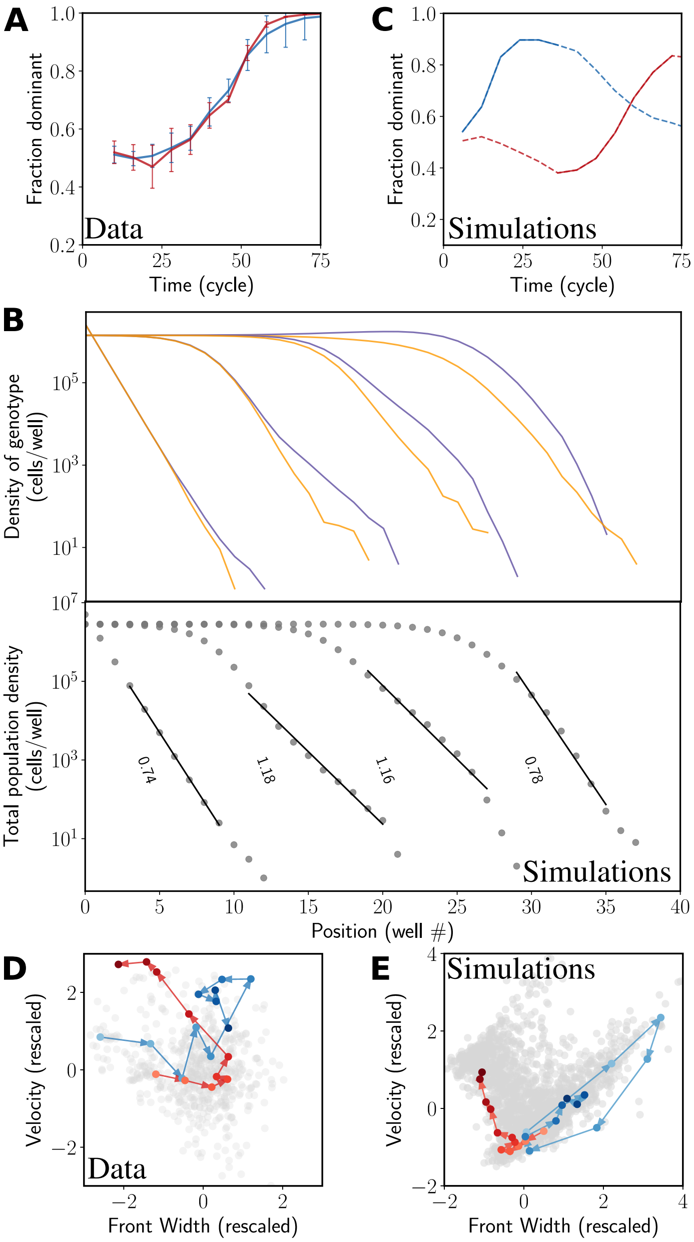
A
Fraction dominant
1.0
0.8
0.6
0.4
0.2
Data
0
25
50
75
Time (cycle)
C
Fraction dominant
Simulations
Time (cycle)
B
Density of genotype (cells/well)
10^5
10^3
10^1
10^7
Total population density (cells/well)
0.74
1.18
1.16
0.78
Simulations
0
5
10
15
20
25
30
35
40
Position (well #)
D
Velocity (rescaled)
2
0
−2
Data
Front Width (rescaled)
E
Simulations
4
Velocity (rescaled)
Front Width (rescaled)
−2
0
2
4

Figure 3-4: **Rapid takeover of the front population by one of the genotypes caused by rare fluctuations of the front can be distinguished from selective sweeps based on the trajectory in the front width - velocity state space A.** In some instances of the expansion experiments, the fraction of one of the species is seen to increase very rapidly. The fraction of the species that eventually dominates is plotted as a function of time for two such instances. Such rapid takeovers are reminiscent of selective sweeps in well-mixed cultures. **B.** During spatial expansions, rapid takeovers can occur without any selection, simply as a result of stochasticity in migration and growth, or rare long distance dispersal. The top panel shows the density of two genotypes in a simulation at different times. In an early cycle, at the very tip, stochasticity in migration led to excess colonization of the purple genotype in a well near the front (jackpot event). This fluctuation then propagated back towards the bulk as the purple genotype rapidly took over the front population. Note how this process was accompanied by a transient widening of the front (bottom panel). **C.** Two instances of rapid takeovers in simulations. The orange curve is from a simulation of a selective sweep during expansion, whereas the blue curve corresponds to a jackpot event. The dotted lines are the entire trajectory, and the solid sections correspond to the takeover times that are analyzed further. **D, E.** Trajectories in the front width-velocity space for experiments (D) and simulations (**E**) corresponding to the solid takeover trajectories in **A** and **C**. Each dot corresponds to the front width and velocity at a single time point for one of the replicates. The axes are rescaled so that the front width and velocity have mean 0 and standard deviation of 1 (to allow for comparison across different environmental conditions) Arrows indicate increasing times. The evolver (orange) in simulations (**E**) first fluctuates around the mean value of the width and velocity. After a while however, a mutant establishes in the front, and the trajectory moves monotonically to the top left after that, towards increasing velocity and decreasing front width. In contrast, for the jackpot event (blue), the front width transiently increases, along with an increase in the velocity, and relaxes back towards the mean velocity and width at later times. Although the timeseries of the fractions in experiments looks nearly identical in the two instances shown, the state space trajectories are clearly distinct. The takeover in the red replicate was due to selection as opposed to a jackpot in the blue replicate.

Appendix A

Appendix to chapter 2

A.1 Materials and methods

A.1.1 Strains

The yeast strain used is the same as the cooperator strain in (58), derived from haploid cells BY4741 [mating type a, European Saccharomyces Cerevisiae Archive for Functional Analysis (EUROSCARF)]. It has a yellow fluorescent protein (yEYFP) expressed constitutively by the TEF1 promoter inserted into the HIS3 locus using the backbone plasmid pRS303.

A.1.2 Experimental protocols

All cultures were grown at 30^oC in standard synthetic media (Yeast Nitrogen Base and Complete Supplement Mixture). The two media used for pulled wave experiments had 0.125% glucose and 0.5% galactose. The media used for studying the transition from pulled to pushed waves consisted of 0.008% background glucose (to reduce the sensitivity of the low-density growth rate to sucrose hydrolysis), in addition to 2%, 0.67%, 0.22%, 0.07%, 0.025%, 0.008%, 0.003% and 0.001% sucrose. All concentrations are wt/vol.

All experiments were performed in $200\mu L$ batch culture in BD Biosciences Falcon 96-well Microtest plates. Migrations and dilutions were performed every 4 hours using the Tecan Freedom Evo 100 robot. Plates were not shaken during growth. Optical densities were measured on the robot before every dilution cycle in the Tecan Sunrise platereader. Cell densities for selected cycles were measured in the MacsQuant flow cytometer after dilution in PBS using the yellow fluorescence channel. Preliminary growth rate measurements on glucose and galactose were performed using overnight optical density measurements every 15 mins. The more sensitive low-density growth rate measurements were performed in 96-well plates without shaking, by measuring initial and final cell densities over 4 dilution cycles, and ignoring the first 2 cycles for to transient effects.

In the analysis, front positions were determined as the interpolated well position where the density (as measured by flow cytometry) crossed a fixed threshold. These were then used to calculate the velocity of expansion. The final velocity was obtained by averaging over multiple thresholds ranging between 100 and 1000 cells per well. The threshold were chosen so as to be sensitive to the dynamics at low density but at the same time not too low to be affected by Poisson errors in cell counts. Spatial decay rates were measured after translating the profiles at different times so that they coincide, and using the combined data to obtain a reliable fit.

A.2 Reaction-diffusion models for one-dimensional range expansions

Populations expanding via short-range migration in one spatial dimension are often modeled as a continuous space, time reaction-diffusion equation:

$$\frac{\partial n}{\partial t} = D\frac{\partial^2 n}{\partial x^2} + ng\left(n\right) \tag{A.1}$$

where $n(x,t)$ is the density of population at position x at time t. D is the dispersal coefficient, which is assumed to be constant in the simple model, and $g\left(n\right)$ is the density dependent per capita growth rate of the population. Many properties of this model can be computed analytically by linearizing the growth term, $ng\left(n\right) \approx ng\left(0\right)$

at low densities (Fig. A-1); we will also denote $g\left(0\right)$ as r_0. This approximation is often accurate because population densities are low at the expansion front. Kolmogorov et. al. proved that, when $g\left(n\right)$ is a monotonically decreasing function, this linearization is guaranteed to capture the expansion dynamics [64]. Expansions described by the linearized growth term are called pulled because they advance via growth at the low-density front, which effectively pulls the waves forward. Importantly, the condition derived by Kolmogorov et al. is sufficient but not necessary. In particular, the linear approximation continues to hold even when a small Allee effect is present. For larger Allee effects, dispersal from the faster growing high density region of the front dominates the growth at the low-density expansion edge, effectively pushing the wave forward. These 'pushed' waves advance at a higher velocity than one would predict using just $g\left(0\right)$ [29].

Although the model (Eqn. A.1) can be analyzed in numerous ways [29, 30, 35], a solution using Fourier transforms is most useful for extending the results to the case of discrete space and time systems, such as in our experiments. Here, we briefly outline the solution to the continuous model using Fourier modes as described by van Saarloos [29]. We then apply a similar analysis to a model appropriate for our experimental system, which was used to predict the linearized-growth-velocities in the main text. The spatial Fourier modes of the front can be written as:

$$\tilde{n}(q,t) = \int_{-\infty}^{\infty} n(x,t) e^{-iqx} dx \tag{A.2}$$

where q is the wave number of the Fourier modes. To obtain the spreading speed of a front, we start with an Ansatz assuming the Fourier modes are of the form $\tilde{n}(q,t) = \tilde{n}(q)e^{-i\omega(q)}t$. Substituting back in eqn. A.1 gives the dispersal relationship $(\omega(q) = i(r_0 - Dq^2))$. Assuming that the front moves with some constant asymptotic velocity, $v^\star$, we perform inverse Fourier transforms in the coordinate frame moving with the front $(\zeta = x - v^\star t)$:

$$n(\zeta,t) = \frac{1}{2\pi} \int_{-\infty}^{\infty} dq \; e^{iq\zeta - i[\omega(q) - v^\star q]t} \tag{A.3}$$

In the large time limit, only those modes near the saddle point of $[\omega(q) - v^\star q]$ survive [90], which results in the following condition:

$$v^\star = \left[\frac{d\omega}{dq}\right]_{q^\star} \tag{A.4}$$

where $q^\star$ is the saddle point. Further, in the commoving reference frame, the wave profile neither grows nor decays in time, so the imaginary part of the exponent must vanish:

$$\Phi(\omega(q^\star)) - \Phi(q^\star)v^\star = 0 \tag{A.5}$$

This gives the set of relationships that can be used to calculate the asymptotic velocity:

$$v^\star = \left[\frac{\Phi(\omega(q))}{\Phi(q)}\right]_{q^\star} = \left[\frac{d\omega}{dq}\right]_{q^\star} \tag{A.6}$$

Using the above two relationships, the asymptotic speed and the exponential decay rate at the front for the F-KPP equation (eqn. A.1) become (note that from eqn. A.3, is seen as the spatial decay rate):

$$v^\star = 2\sqrt{r_0 D},\ \lambda = \sqrt{\frac{r_0}{D}} \tag{A.7}$$

A.3 Expansions in discrete space and time models

The discretized form (corresponding to the experimental protocol) of the F-KPP equation can be written as:

$$n_{x,t+\Delta t} = g_{\Delta t}\left(n_{x,t} + \frac{m}{2}\left(n_{x+\Delta x,t} + n_{x-\Delta x,t} - 2n_{x,t}\right)\right) \tag{A.8}$$

where x is the spatial coordinate, and t is the cycle number. $g_{\Delta t(n)}$ is the per capita growth rate, which upon linearization can be written as:

$$g_{\Delta t}(n) = n\frac{e^{r_0 \Delta t}}{dilution} \tag{A.9}$$

corresponding to exponential growth at rate r_0 followed by a dilution. Substituting the Fourier mode $\tilde{n_x} = e^{iqx - i\omega t}$ in the above linearized equation gives the dispersion relation:

$$e^{-i\omega \Delta t} = \frac{e^{r_0 \Delta t}}{dilution}\left[1 + m\left(cosh(-iqx) - 1\right)\right] \tag{A.10}$$

Following the analysis of the continuous case, we use saddle point approximation and require that the front is not changing in the commoving reference frame. The resulting equations are equivalent to requiring that $v(\lambda) = s/\lambda$ is minimized over λ. Here, $\lambda = \Phi(q),\ s = \Phi(\omega)$. For small Δt, the corrections can be derived analytically by Taylor expansion. However, since in our experiments, $\Delta t = 4$ hrs, which is longer than the time scale set by the growth rate (2 hrs), the velocity and spatial decay rate for the discretized system cannot be calculated as small corrections to the continuous solution, but have to be evaluated by minimizing eqn. A.10 numerically.

The magnitude of these corrections from the continuous model are shown in Fig. A-3. Note that the discretized dynamical equation corresponding to the experiment is not the same as the discretized version of the F-KPP equation, which can be written as:

$$n_{x,t+\Delta t} = n_{x,t}e^{r_{0,eff}\Delta t} + D_{eff}\frac{\Delta t}{\Delta x^2}\left(n_{x+\Delta x,t} + n_{x-\Delta x,t} - 2n_{x,t}\right) \tag{A.11}$$

Comparing this with the experiment, the effective growth and diffusion rates in the continuous space-time model can be written in terms of experimental parameters as:

$$\begin{aligned} r_{0,eff} &= r_0 - \frac{ln(dilution)}{\Delta t} \\ D_{eff} &= \frac{m}{2}\frac{\Delta x^2}{\Delta t}(1 + r_{eff}\Delta t) \end{aligned} \tag{A.12}$$

($\Delta t = 4$ hr, $\Delta x = 1$ well). The effective parameters can then be used in continuous models to compare them to the discrete space-time experimental model and evaluate the magnitude of 'corrections' that are introduced due to the discretization.

The finite number of organisms per spatial patch also changes the velocity and spatial decay rate. Although stochastic effects obviously cause fluctuations in the velocity, the expectation value of the velocity is also reduced as compared to predictions that do not incorporate demographic stochasticity. The deviations have been shown to be of the order of $1/log^2 N$, where N is the number of individuals per unit length, when space and time are continuous [63]. Moreover, the fronts have been shown to be steeper when demographic stochasticity is added [62, 63]. We see this in our experiments, where, without accounting for the demographic stochasticity, the observed spatial decay rate is larger than predicted. This discrepancy vanished when we incorporated the effects of stochasticity in our predictions (Fig. A-4).

A.4 Cubic model of the Allee effect

A generic model of the Allee effect was used for making the cartoon in Fig. 4 in the main text. In this model, the density dependence of growth is given by:

$$\frac{1}{n}\frac{dn}{dt} = \frac{r_0}{a}\left(1 - \frac{n}{k}\right)(n + a) \tag{A.13}$$

This model shows no Allee effect for $a > k$ (per capita growth rate monotonically decreases with increasing density), and a weak Allee effect for ($a < k$). Further, as a is varied, the growth rate at low density remains constant and is given by r_0. The transition from pulled to pushed waves occurs at $a = k/2$ inside the weak Allee effect regime [35].

A.5 A mechanistic growth model captures the Allee effect and shows a transition from pulled to pushed waves with increasing sucrose

We developed a mechanistic model for yeast growth in our experiments. The model incorporates previously well-studied mechanisms such as Monod growth on glucose [91] and a Michaelis-Menten kinetics of sucrose hydrolysis [59, 61, 92]. Using previously measured values of the model parameters A.1, we found that the magnitude of the Allee effect increases with the amount of sucrose in the medium. Importantly, the model also displayed a transition from pulled to pushed waves, consistent with the experimental observations in Fig. 2-5 (Fig. A-7). This transition was observed for a wide range of model parameters and is a generic prediction of the model. To test for quantitative agreement between the model and the experiments, we fitted the parameters of the model to our independent measurements of the growth rates, and confirmed that the predicted velocities closely match experimental observations (Fig. A-8).

The model describes growth of yeast in the presence of glucose and sucrose, and assumes that there are no other limiting resources. Furthermore, while glucose is metabolized directly by the yeast, sucrose needs to be hydrolyzed to monosaccharides before it can be utilized. Although sucrose is hydrolyzed to glucose and fructose, we treat these sugars equivalently and refer to the combined concentration of the monosaccharides as the glucose concentration [59]. This hydrolysis reaction is catalyzed by an enzyme invertase produced by yeast cells. Most of the invertase stays attached to the cell surface resulting in higher rates of hydrolysis in the immediate vicinity of the cell and creating a local cloud of glucose in excess of the bulk glucose concentration. Thus, yeast cell benefit from both the glucose produced by themselves and from the glucose produced by their neighbors [59]. These dynamics are captured by the following Monod growth law and glucose consumption equation:

$$\frac{1}{n}\frac{dn}{dt} = \frac{g_{loc}}{g_{loc} + k_g}\gamma_{max} \tag{A.14}$$

$$\frac{dg}{dt} = -Y\frac{dn}{dt} + nV \tag{A.15}$$

Here, the first equation describes cell division, where n is the cell density, g_{loc} is the local glucose concentration around each cell, k_g is the Michaelis-Menten constant for glucose utilization and γ_{max} is the maximum division rate. The second equation gives the corresponding rate of utilization of glucose (g), which is proportional to the division rate of the cells (the proportionality constant, Y, determines the carrying capacity of the population). The additional term, nV, corresponds to the production of glucose due to sucrose hydrolysis. The per capita rate of sucrose hydrolysis, V, is given by

$$V = v_s\frac{s}{s + k_s} = -\frac{1}{n}\frac{ds}{dt} \tag{A.16}$$

where s is the sucrose concentration, v_s is the maximum rate of sucrose hydrolysis, and k_s is the Michaelis-Menten constant. Finally, the local glucose concentration around the cell is the sum of the bulk glucose concentration, and the additional cloud of glucose due to the sucrose hydrolysis on the cell surface. The contribution of this cloud is proportional to the rate of sucrose hydrolysis, and thus

$$g_{loc} = g + g_{eff}V \tag{A.17}$$

where g_{eff} is the proportionality constant that accounts for the glucose escape through diffusion [59].

To infer model parameters, we measured growth rates in varying sucrose concentrations, and different cell densities. The growth rate measurements and the corresponding range expansions were carried out in 9 different media: 0.125% glucose, and 0.008% glu + varying amounts of sucrose.

Before we describe the specifics of how the model parameters were determined from the experimental data, it is important to discuss how each parameter contributes to the different aspects of the experimental data and demonstrate that the data contains sufficient information to constrain the model parameters. The yield parameter, Y, determines the number of cells that can be produced given a certain amount of glucose. For the growth rate measurements in pure glucose, Y therefore controls the population densities at which the growth rate precipitously drops to zero. We determined Y by fitting the model prediction to our growth measurement at high cell densities in 0.125% glucose (Fig. A-9). The growth rate at low cell densities in pure glucose media is completely determined by γ_{max} and k_g, and our data contained sufficient information to infer these parameters because we had low-density growth rate measurements in pure glucose as well as in several sucrose concentrations that produced varying local concentrations of glucose as specified by eqn. A.17. The low-density growth rates at different sucrose concentrations also depend on k_s and $v_s g_{eff}$; therefore, we could use our low-density measurements to infer four model parameters $\gamma_{max}, k_g, k_s, v_s g_{eff}$.

The dynamics at high population densities depend not only on the product of v_s and g_{eff}, but on the individual values of these parameters. In particular, higher values of v_s and lower values of g_{eff} (keeping their product fixed) result in a larger Allee effect and more cooperative growth because of the faster sucrose hydrolysis and greater sharing of glucose via diffusion away from the cell. Therefore the magnitude of the Allee effect at high sucrose concentration provided the last necessary constraint to determine all of the model parameters.

Instead of directly fitting to the entire data set simultaneously, we used a modular approach of fitting the growth dynamics at low-density and high-density separately. We also bootstrapped on our data to determine the uncertainty in model parameters and model predictions.

To obtain a set of low density growth parameters, we bootstrapped over the measured values of growth rates in each of the media, and fitted the parameters by minimizing the squared distance from the bootstrapped data using Python package scipy (curve_fit). All data at starting densities below OD 0.004 was included, as indicated in Fig. A-10. However, all outliers more than 2.5 SD away from the mean, were excluded from the analysis. Moreover, growth was unusually slow in one of the measurements, in 0.003% sucrose. This is the regime where the low-density growth rate is independent of sucrose concentration, since the concentration of sucrose is lower than that of glucose, which was 0.008%. Therefore, we excluded this particular condition while fitting the parameters. The bootstrapping procedure was repeated to obtain 100 sets of low-density growth parameters, $\gamma_{max}, k_g, k_s, v_s g_{eff}$. Out of these, a few iterations of the curve_fit routine did not converge on the fit, leaving 89 sets of parameters for downstream analysis. Fig. A-11 shows the low-density growth rates that the model predicts for each of the parameter sets.

Next, for each of the 89 sets obtained above, we determined the individual parameters, v_s and g_{eff}, keeping the product constant. As noted earlier, the relative magnitudes of these two parameters control the magnitude of the Allee effect. Therefore, parameters v_s and g_{eff} were determined by minimizing the squared distance from growth rates at intermediate densities in 2%, 0.67% and 0.22% sucrose – the media that exhibit a substantial Allee effect. The sum of squared distance from all the data points in the selected regions of the cell densities was calculated for values of ranging from 0.2 to 4 % $\mathrm{OD}^{-1}\mathrm{hr}^{-1}$, and the value of v_s minimizing the sum was chosen. These regions of cell densities were selected such that the growth rates increase with density (i.e. exhibit an Allee effect) and are summarized below:

2% sucrose: OD 5×10^{-3} to 2×10^{-1},

0.67% sucrose: OD 5×10^{-3} to 2×10^{1},

0.22% sucrose: OD 5×10^{-3} to 3×10^{-1}.

Table A.1 shows a comparison between the previously reported values of the parameters for yeast, and the median parameter values that we have obtained by the procedure described above. The distribution of parameter values is shown in Fig. A-12. Most of the fitted values were consistent with literature. The exception is g_{eff}, which is an order of magnitude larger than previously reported. However, this parameter depends strongly on the diffusion rate of glucose, such that slower diffusion leads to larger g_{eff}. Since the cells in our experiments are not being shaken (both during range expansions as well as in the experiments we performed to measure growth rates), most of the hydrolysis products remain in the vicinity of the cell, resulting in lower diffusion, and a larger g_{eff}. Other factors that affect g_{eff} such as genetic background, cell size, etc. could also contribute to the observed difference with previous measurements. The lack of mixing is also consistent with the slightly lower v_s that we estimate compared to literature, since the efficiency of hydrolysis is reduced.

These 89 parameter sets fit the observed growth rates well over the entire range of cell densities and sucrose concentrations as shown in Fig. A-13.

We then simulated expansions using the mechanistic growth model and the 89 parameter sets obtained above. The simulated velocities for each of the 89 parameter sets all show a transition from pulled to pushed waves with increasing sucrose concentration, and are distributed closely around experimentally observed velocities (Fig. A-8).

The excellent agreement between the model and the experimental observations further supports our conclusions that the break-down of the theory of pulled waves at high sucrose concentrations is due to an increasing strength of the Allee effect makes yeast expand as a pushed wave.

A.6 Simulations

Stochastic simulations were performed for computing the rate of exponential density decay at the front as well as for testing the predictions of the mechanistic growth model. In the simulations, the expansions were allowed to proceed for longer times than in the experiment, so as to completely remove all transients. Expansions were typically simulated for 60 cycles across a sufficiently long landscape so that the waves do not reach its edge. The total carrying capacity in each spatial patch was the same as in the experiments.

The simulations reflect exactly dynamics in our experiments (Fig. A-14). The cells start with an exponential spatial density profile. For each cycle, logistic model (in simulations for calculating the exponent at the front) or the mechanistic growth model is integrated over a period of 4 hours to obtain the final population density in each well. Growth is thus deterministic in the simulations. At the end of the growth cycle, the number of cells is rounded off to the nearest integer. Binomial sampling is used to determine the number of cells that are transferred for the next cycle, taking into account the migration rate as well as the dilution rate. This step therefore accounts for the demographic fluctuations.

Finally, since growth in the mechanistic model explicitly depends on sugar concentrations, we also include the effects of sugar transfer due to migration and dilution in the simulations.

Velocities in the simulations are calculated in the same way as experiments (Section A.1). A threshold density of 2000 cells per well and the location of the wavefront is defined as the position at which the profile crosses this threshold. Velocity is then calculated by obtaining a linear fit between the position and time.

A.7 Supplementary figures

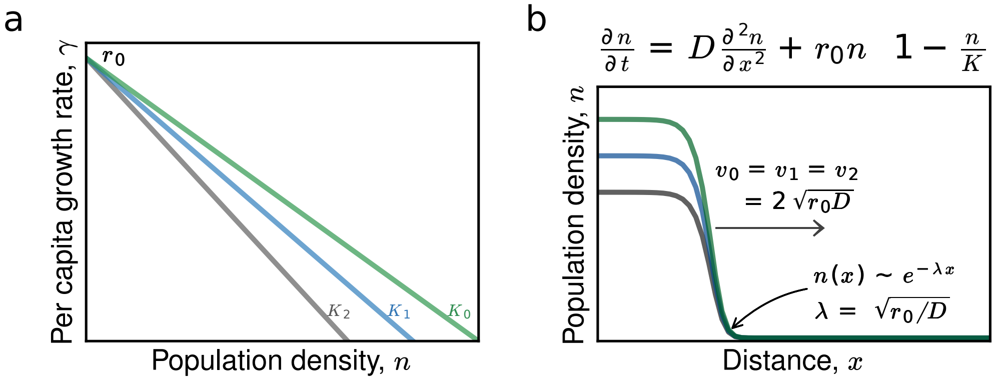

Figure A-1: Reaction-diffusion equations are classical models for expansion in theoretical ecology. When populations grow logistically, Fisher's equation predicts traveling waves of constant velocity, with an exponential spatial profile near the front. Both of these emergent properties depend only on the low-density growth rate, and are independent of the carrying capacity. (a) Populations that obey logistic growth increase exponentially with rate r_0 at low density, and the per capita growth rate decreases monotonically until the population density saturates at some carrying capacity, K. Three growth curves with identical low-growth rate, but different carrying capacities are shown. (b) Emergent properties of the expansion front, such as velocity (v) and spatial decay rate of density at the front (λ), depend only on the per capita growth rate at low density (r_0) and the diffusion constant (D), and are independent of the carrying capacity ($v_0 = v_1 = v_2$, $\lambda_0 = \lambda_1 = \lambda_2 = \lambda$). The bulk density, however, does depend on the carrying capacity (K).

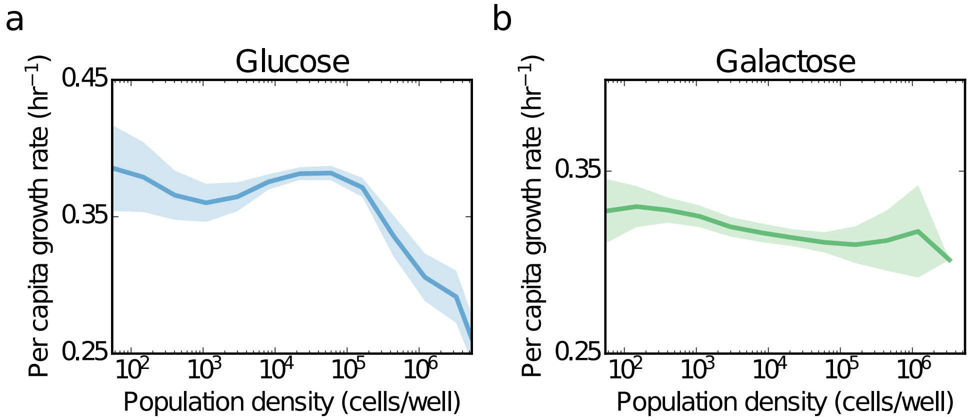

Figure A-2: The maximal per capita growth rate in galactose (a) and glucose (b) never significantly exceeds the per capita growth rate at low density. We measured the fold growth by counting the number of yeast cells before and after 4 hours of growth in a 96-well plate. Each well started with a small number of yeast cells. After propagating the cultures with dilution for two 4-hour cycles (to remove transient effects caused by a change of growth environment), the number of cells in the wells were counted by flow cytometry at the beginning and end of the third and fourth cycle. Cells were counted after diluting by 100x. Due to the small numbers, the actual counts at low density had a large sampling noise. The figure shows the growth rate as an average over a Gaussian moving window. Shaded region indicates standard deviation in the average over the window in bootstrapped data. Since density doesn't change much over the course of four hours, growth rate was estimated from the fold growth by assuming exponential growth at a constant rate.

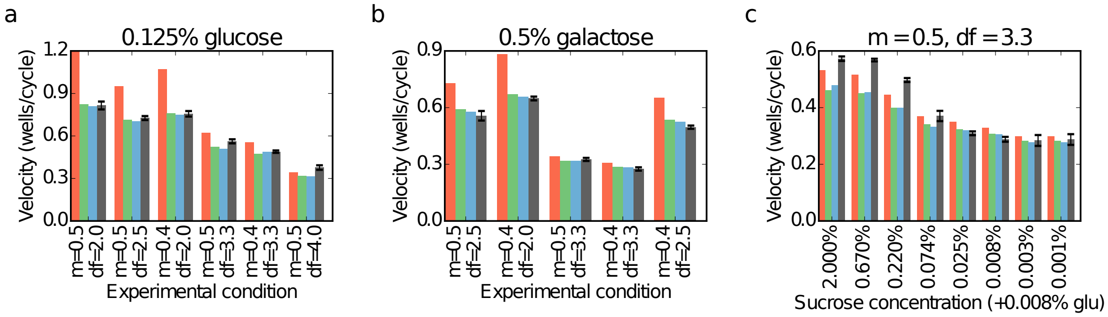

Figure A-3: Effect of discretizing space and time (and addition of demographic stochasticity) on predicted velocity in glucose (a), galactose (b) and sucrose (c) environments. Each set of bars represents an experimental condition (different migration and death rates). In (c), the 8 conditions have constant migration and death rate, but decreasing amount of sucrose starting with 2% in condition 1 to 0.001% in condition 8. Red bars indicate predicted Fisher velocities in continuous space-time models with the same effective growth and diffusion rate as the discrete experimental system (SI eqn. A.12). Here, we show a decomposition of the effects due to discrete space-time, and demographic stochasticity. Discreteness of space and time (green): Since migration is limited to one well at a time in the linear stepping stone model, emergent wave velocities can never exceed 1 $well/cycle$. For short cycles (on the time scale set by the growth rate), these corrections can be approximated analytically. For the 4 hour experimental discretization, however, the corrections are large, and have to be calculated numerically (SI eqn. A.10). Demographic stochasticity (blue): Demographic stochasticity has been predicted to reduce expansion velocity. The correction to the continuous space-time model due to demographic stochasticity is of the order of $1/log^2(N)$. In our experiments, we calculated the corrections using simulations with measured growth rates and other known experimental parameters. Experimental data (gray): We see that the observed velocities are in close agreement with predictions once the effects of discretization and stochasticity are incorporated (subplots a, b). Subplot (c) shows data for expansions in sucrose, where the observed velocities are much larger than predicted velocities (even after incorporating the effects described above). Conditions 1 through 8 correspond to sucrose concentrations starting from 2%, decreasing by a factor of 3 in consecutive conditions. Thus, observed velocities are close to predictions for condition 5 onwards, when the Allee effect is no longer sufficiently strong. Error bars indicate S.D. in measured velocity at five different threshold densities.

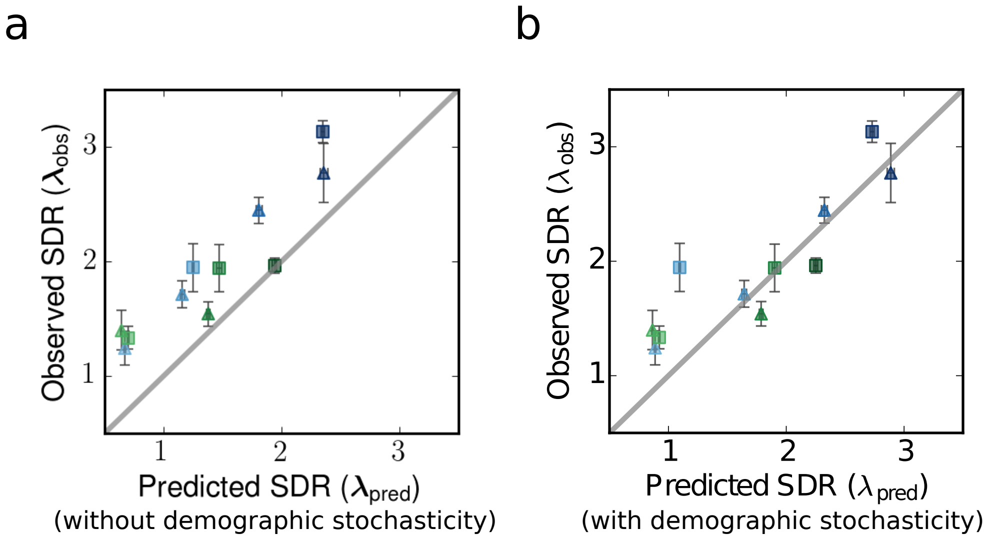

Figure A-4: Demographic stochasticity significantly affects the spatial decay rate at the front. (a) Predicted spatial rate of decay at the front, based on linearized growth, is less than what is experimentally observed when demographic stochasticity is not taken into account. (b) When finite population effects (demographic stochasticity) are included, the observed front shape is close to predictions. The predicted spatial decay rate is based on simulations using measured values of low-density growth rate and known experimental parameters such as migration and death rate. y-axis error bars indicate S.D. in measured decay rate for three different fitting regions at the front.

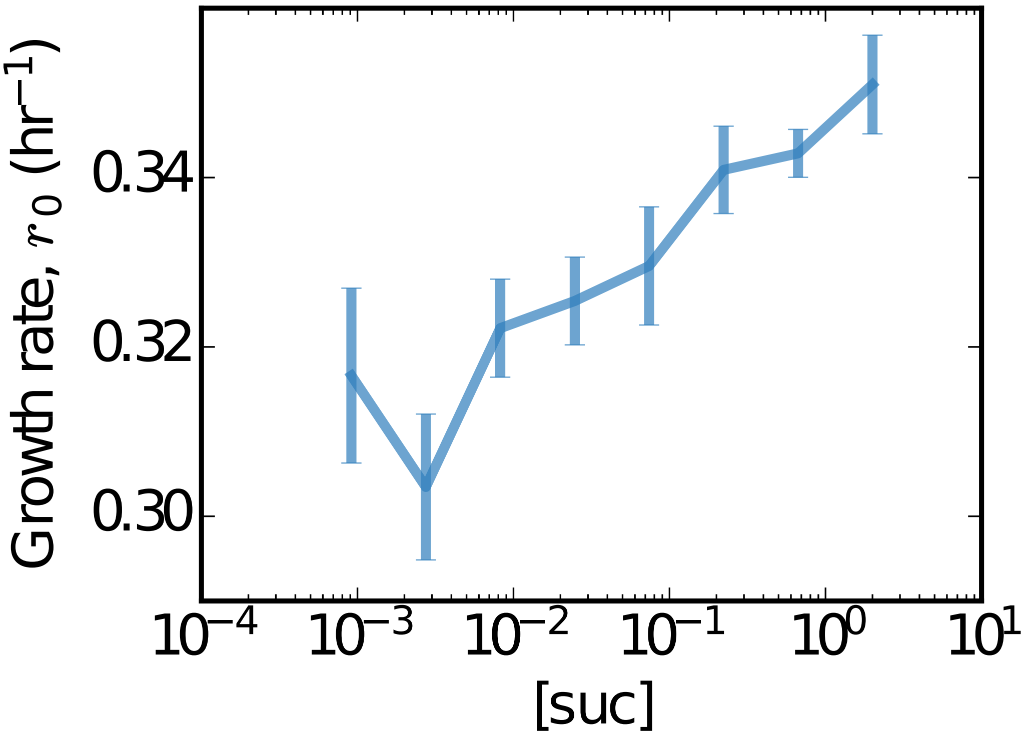

Figure A-5: **Low density growth rate increases slowly with increasing sucrose concentration.** Since some of the hydrolyzed sucrose is captured by the yeast cells before it can diffuse away, increasing the sucrose concentration leads to increased growth rates even at low densities, when cooperative effects are absent (section)A.50. However, the maximal growth rate increases faster than the low density growth rate, resulting in an increasingly severe Allee effect (Fig. A-6). Error bars represent SEM in measured low density growth rates (Fig. A-10).

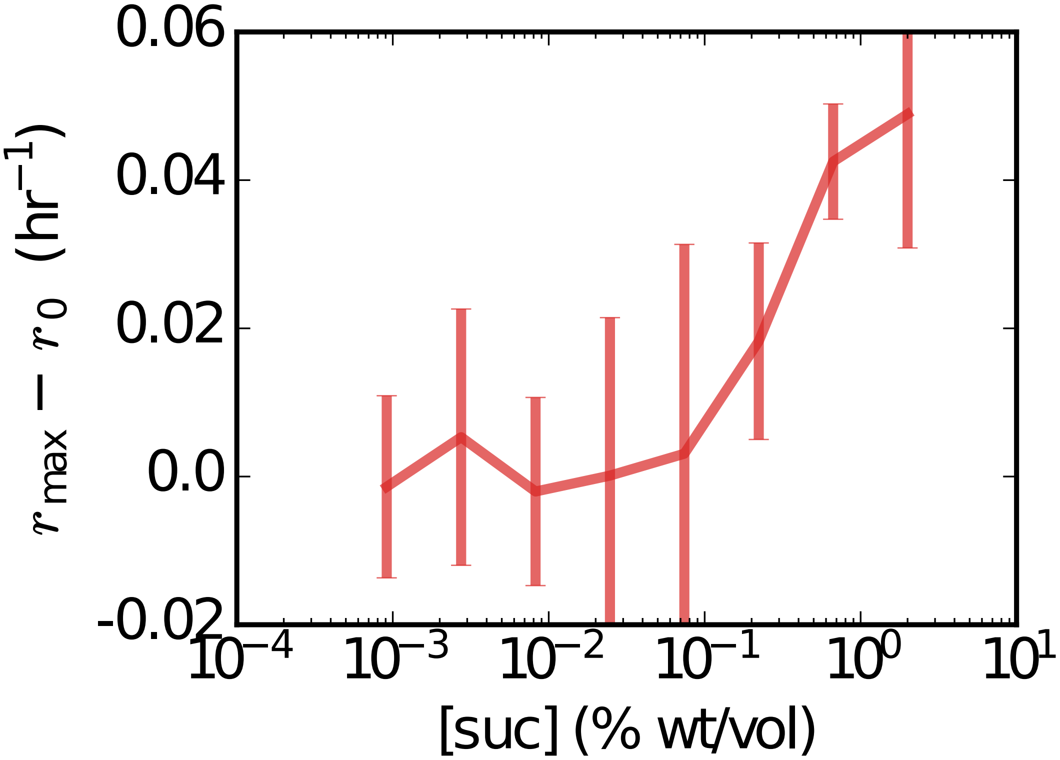

Figure A-6: **Magnitude of Allee effect increases with increasing sucrose concentration.**. The magnitude of the Allee effect is estimated as the difference between the maximal growth rate, r_{max} and the low density growth rate, r_0. Error bars indicate SEM of low-density growth rate, (Δr_0). r_{max} was determined as the maximal value of the growth rate after averaging over a moving Gaussian window as shown in Fig. A-2 for 0.125% glucose and 0.5% galactose.

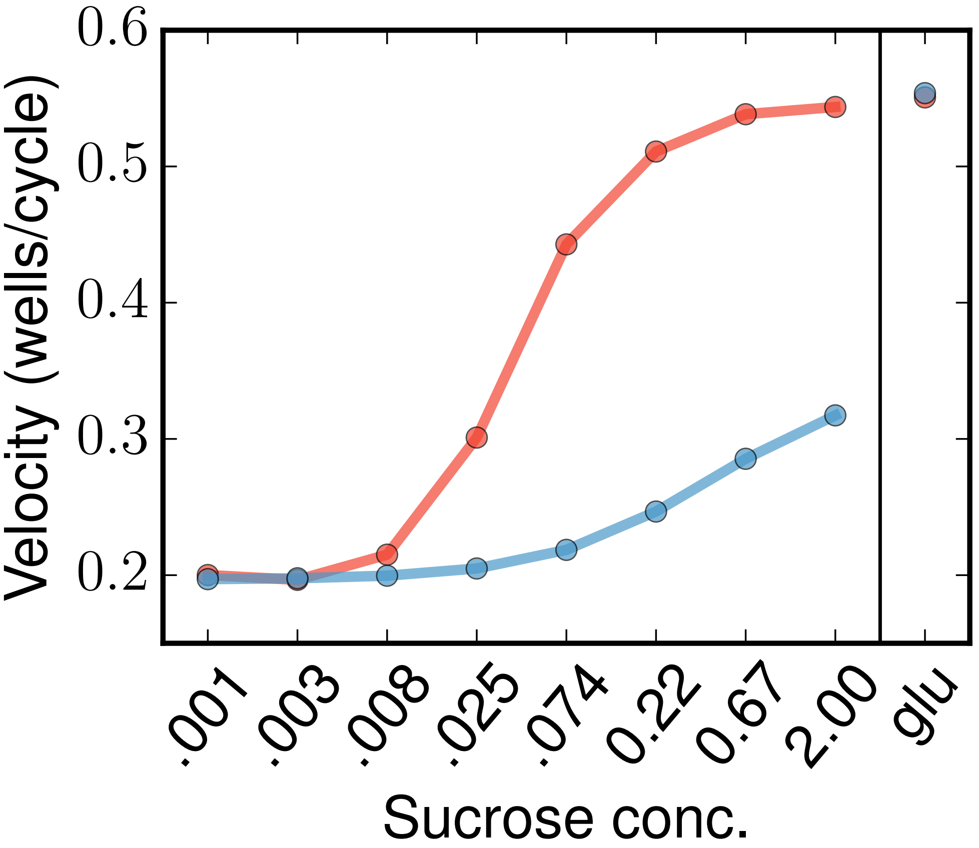

Figure A-7: **A mechanistic model of yeast growth on sucrose and glucose predicts a transition from pulled to pushed waves (Section A.5).** A simple mechanistic model where yeast grows on glucose following Monod kinetics, and hydrolyzes sucrose to glucose (section A.5) was used to simulate expansions. All the parameters in the model have been reported previously in various studies. Using typical parameter values from published literature (Table A.1), the model predicts a transition from pulled to pushed waves as the sucrose concentration in the media is increased. At low sucrose concentrations, expansions are pulled, reflected in the agreement between simulated velocities and linearized-growth predictions. At larger sucrose sucrose concentrations, expansion velocities exceed the linearized-growth prediction, indicating that the expansions are pushed.

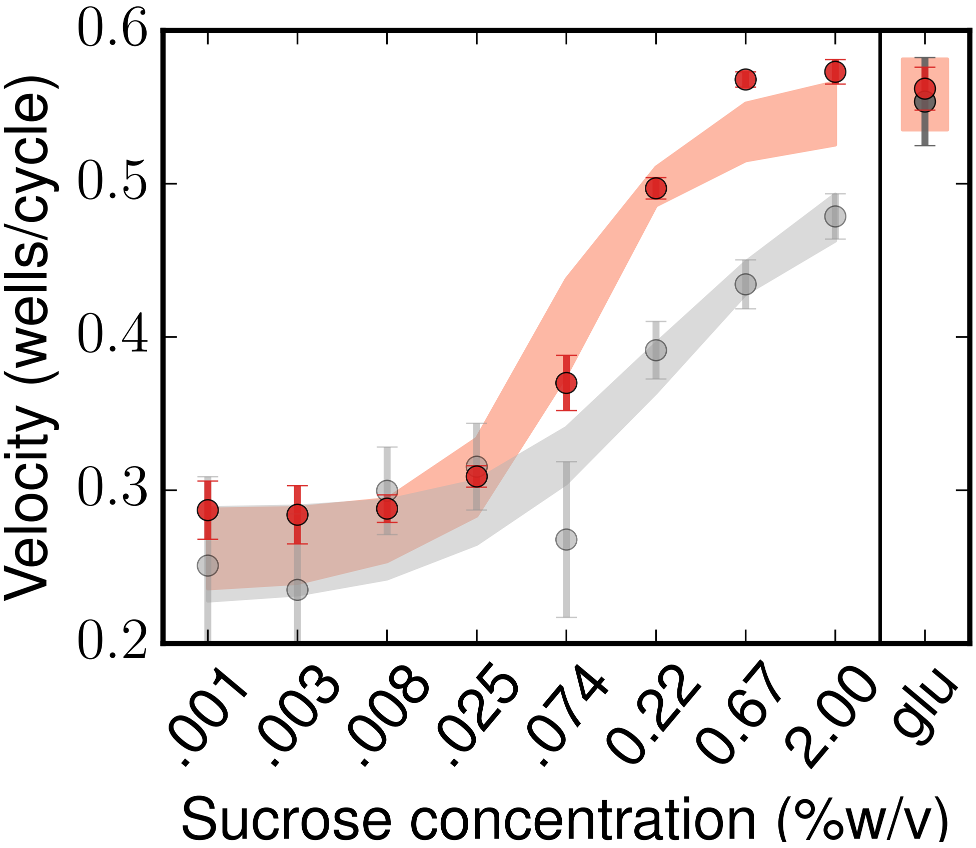

Figure A-8: A mechanistic model for growth on glucose and sucrose predicts velocities close to what are observed experimentally. Experimentally observed velocities in 8 different sucrose concentrations and in 0.125% glucose are shown as red points with SD errorbars. Gray points show the predicted linearized-growth velocities. Error bars are obtained by bootstrapping on the measured growth rates at low densities and calculating the linearized growth velocities. Shaded regions indicate predictions of the model. The observed velocities match well with the predictions of the model. The model also captures the transition from pulled to pushed waves as the deviation between observed and linearized-growth velocities (gray shading) around sucrose concentrations of around 0.025%. The width of the shaded regions is the standard deviation of simulation results for 89 parameter sets obtained by bootstrapping over the growth rate measurements and fitting the model to the bootstrapped data.

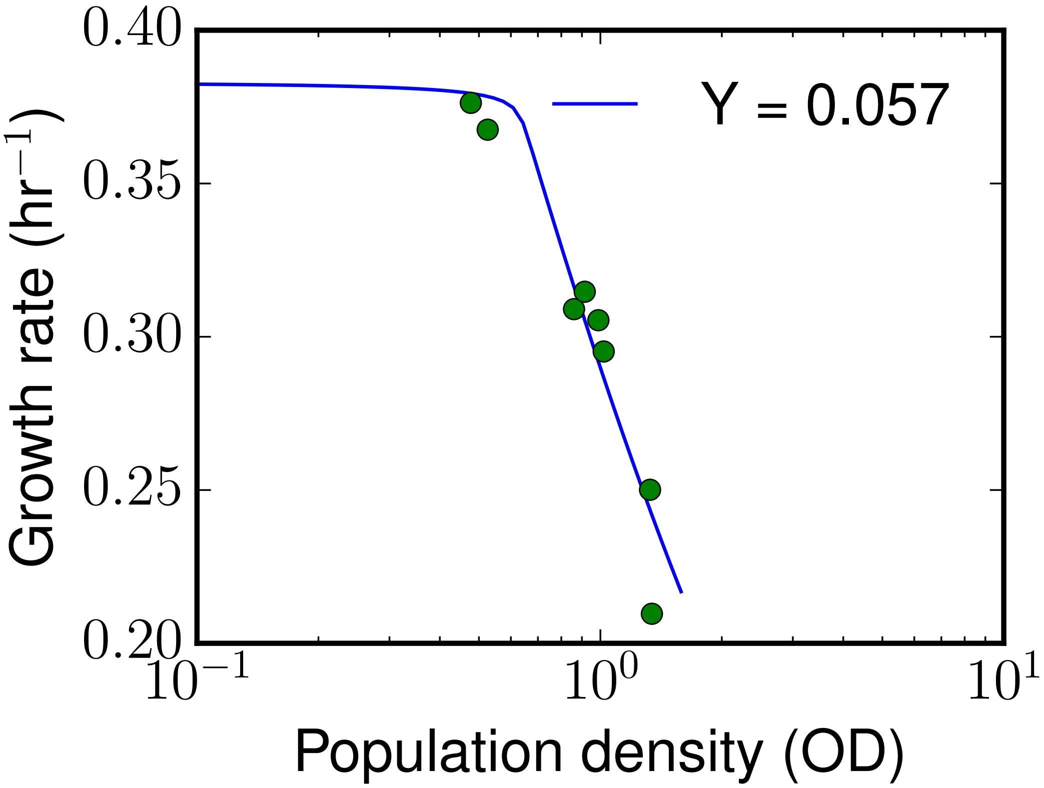

Figure A-9: The yield parameter in the mechanistic model, Y, was obtained by fitting the model to growth rate measurements in 0.125% glucose, at high densities, where there is a sharp decrease in growth rate with density. The yield parameter reflects the amount of glucose that a cell utilizes per division. At high cell densities, glucose is depleted quickly causing the per capita growth rate to decrease sharply as starting OD is increased. By fitting the model to this region of growth, the value of Y can be determined accurately: $Y = 0.057 OD^{-1}$. Data is shown as green points, only at high densities, where growth rate is strongly affected by the yield parameter due to resource limitation.

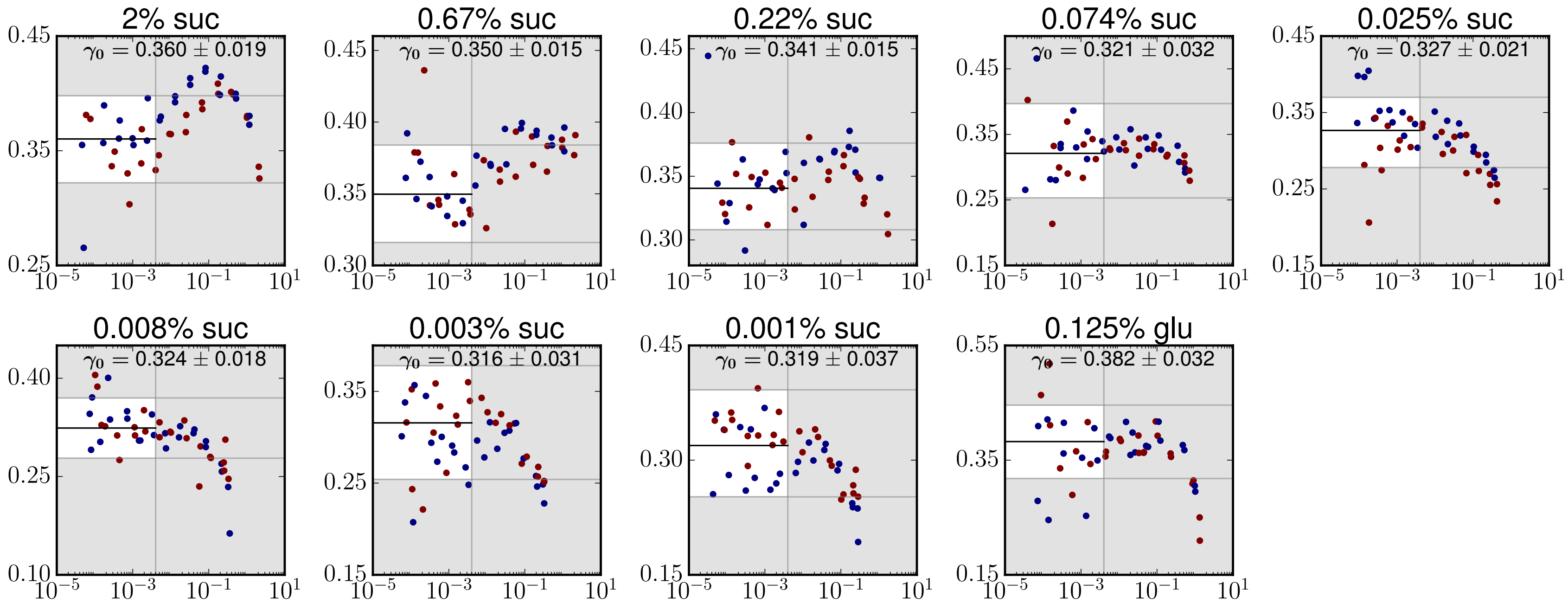

Figure A-10: Low density growth rates were measured by averaging the growth rate measurements over densities up to OD 0.004 (corresponding to 1000 cells per well). Population density is plotted along the x-axis, in terms of OD600, and growth rate is plotted along the y-axis for each panel. Data in the unshaded region is included as growth rate at low density. this region includes all data at ODs below 0.004 except for the outliers that are more than 2.5 SD away from the mean. Inset text indicates mean and SEM of the unshaded data in hr^{-1}.

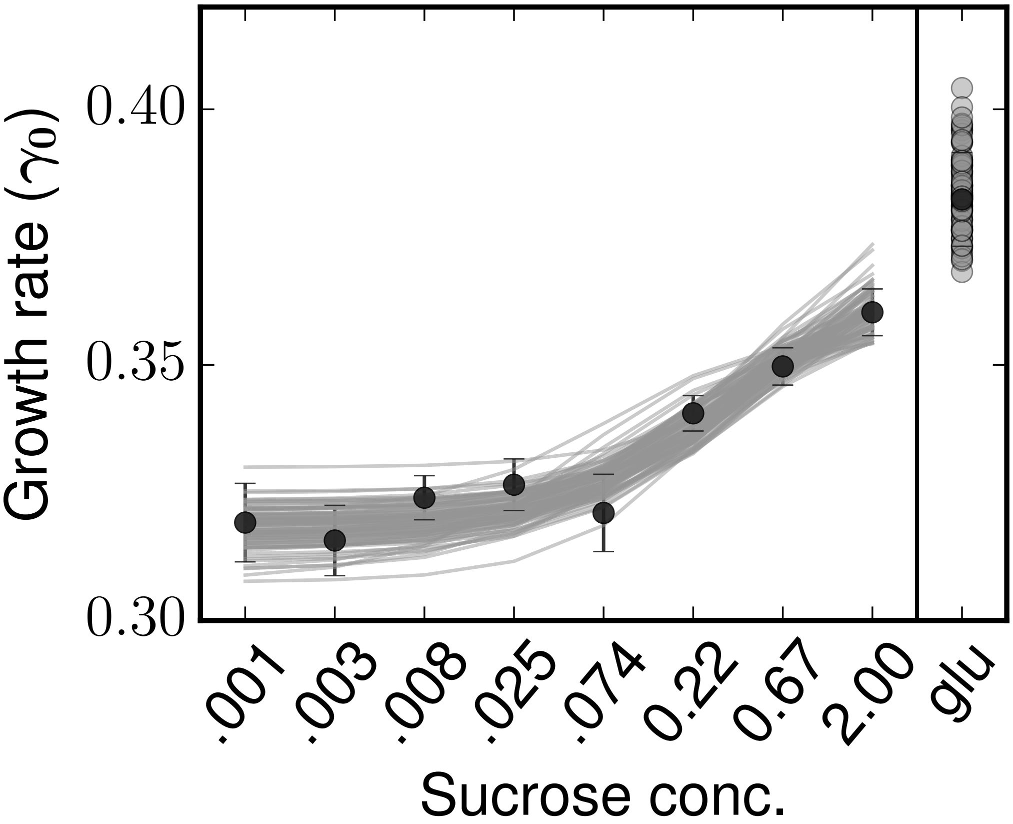

Figure A-11: Low-density growth rates predicted across different sucrose concentrations by the model. We used 89 low-density parameter sets ($\gamma_{max}, k_g, k_s, v_s g_{eff}$) obtained by fitting to bootstrapped low-density growth rate measurements. Black circles with error bars represent the mean growth rate and SEM. Gray lines are model predictions. The details of the bootstrapping procedure can be found under section A.5.

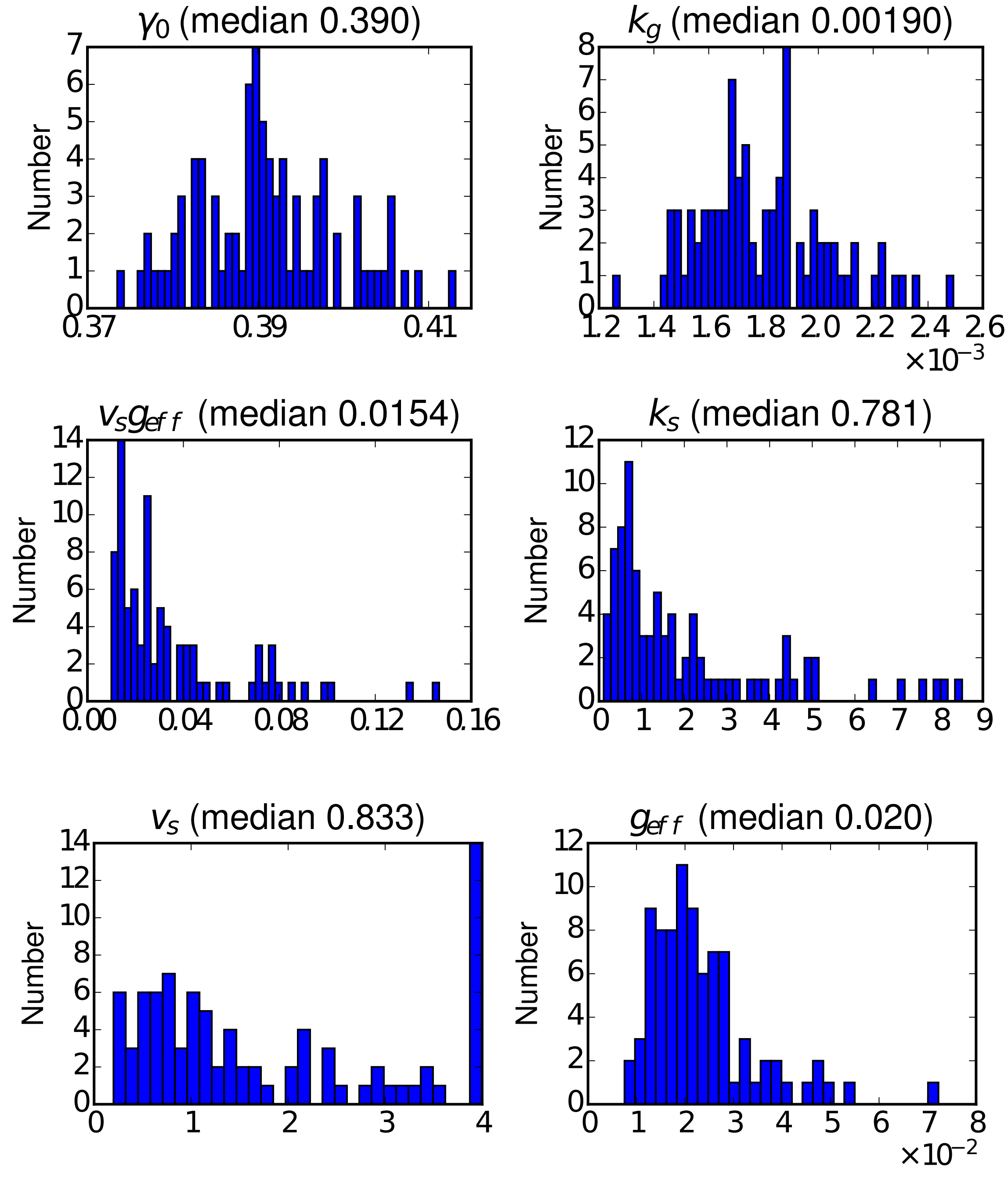

Figure A-12: Distribution of parameter values in the 89 independent parameter sets obtained by bootstrapping over the data. Median values of the parameters are indicated in the title. Most median parameter values are in close agreement with previously reported values in the literature (Table A.1). The exception is g_{eff}, which is expected to differ because the media is not shaken in our experiments (section A.5).

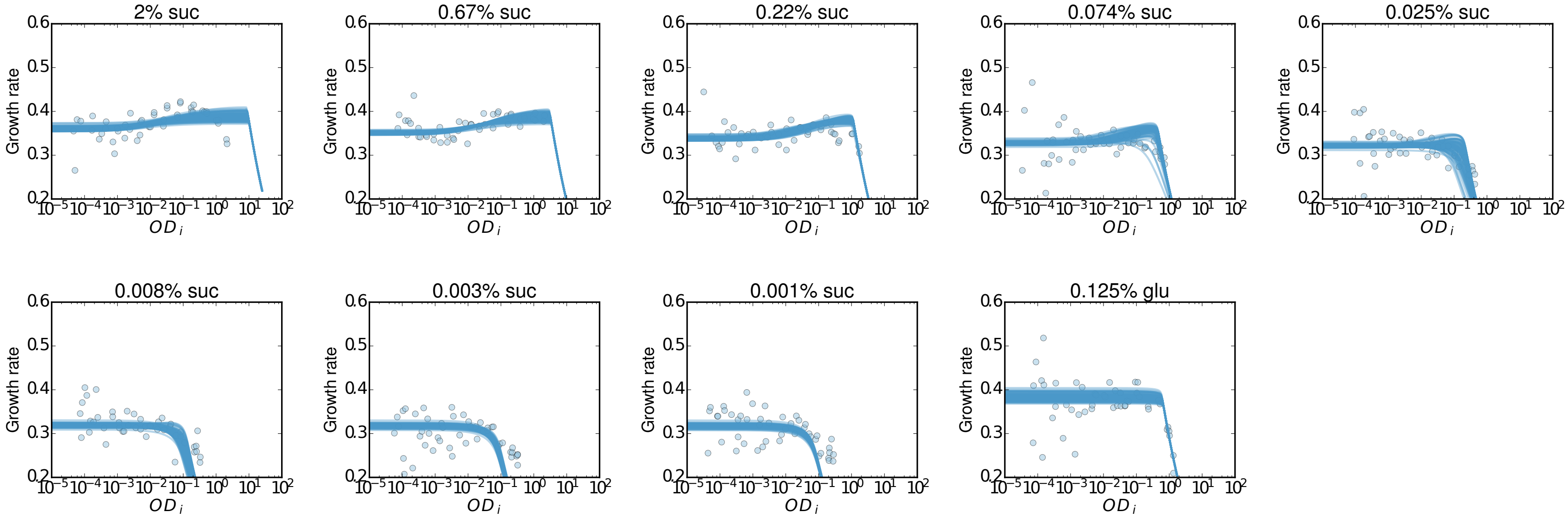

Figure A-13: Allee effect increases with sucrose concentration. Measured growth rates at various cell densities are shown as blue points. Blue curves are the predictions of the model for each of the 89 parameter sets. For all parameter sets, the model matches the data well and shows an increasing Allee effect as sucrose concentration is increased.

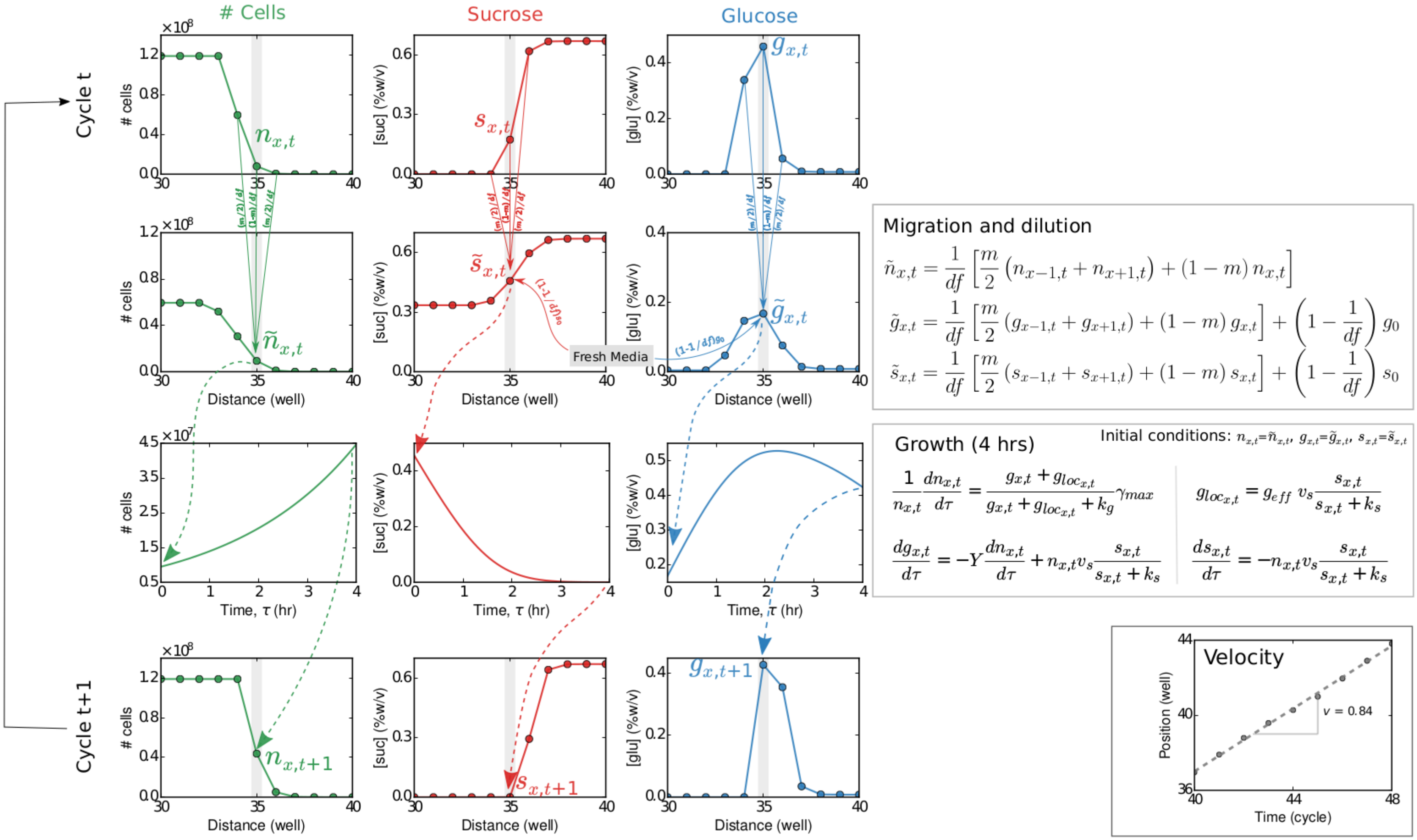

Migration and dilution

$$\tilde{n}_{x,t} = \frac{1}{df}\left[\frac{m}{2}\left(n_{x-1,t} + n_{x+1,t}\right) + (1-m)\,n_{x,t}\right]$$

$$\tilde{g}_{x,t} = \frac{1}{df}\left[\frac{m}{2}\left(g_{x-1,t} + g_{x+1,t}\right) + (1-m)\,g_{x,t}\right] + \left(1 - \frac{1}{df}\right) g_0$$

$$\tilde{s}_{x,t} = \frac{1}{df}\left[\frac{m}{2}\left(s_{x-1,t} + s_{x+1,t}\right) + (1-m)\,s_{x,t}\right] + \left(1 - \frac{1}{df}\right) s_0$$

Growth (4 hrs)

Initial conditions: $n_{x,t}=\tilde{n}_{x,t},\ g_{x,t}=\tilde{g}_{x,t},\ s_{x,t}=\tilde{s}_{x,t}$

$$\frac{1}{n_{x,t}}\frac{dn_{x,t}}{d\tau} = \frac{g_{x,t} + g_{loc_{x,t}}}{g_{x,t} + g_{loc_{x,t}} + k_g}\gamma_{max}$$

$$g_{loc_{x,t}} = g_{eff}\ v_s \frac{s_{x,t}}{s_{x,t} + k_s}$$

$$\frac{dg_{x,t}}{d\tau} = -Y\frac{dn_{x,t}}{d\tau} + n_{x,t}v_s\frac{s_{x,t}}{s_{x,t} + k_s}$$

$$\frac{ds_{x,t}}{d\tau} = -n_{x,t}v_s\frac{s_{x,t}}{s_{x,t} + k_s}$$

Figure A-14: The figure shows how the density of cells and sugar concentrations as a function of space change over a cycle, in the simulation, following the dynamics in a single well highlighted above. At the end of cycle t, the cell density has a certain spatial profile (row 1). At the beginning of cycle $t+1$, cells are diluted by a factor df and at the same time, a small fraction $(m/2)$ is transferred to the neighboring wells (row 2). The exact factor by which the densities change is illustrated next to the arrows from row 1 to row 2. The residual glucose and sucrose in the wells is also transferred over along with the cells. The fresh media into which the cells are diluted contains additional sugars (concentrations s_0, g_0) for the cells to grow. Concentrations and cell densities at this intermediate step are denoted by $\tilde{n}, \tilde{g}, \tilde{s}$. The cells are then allowed to grow for 4 hrs (row 3). In the simulations, the density at the end of 4 hrs is obtained by integrating the growth model starting from the intermediate densities. Thime within the growth phase is denoted by τ. The mechanistic model of growth, involving the cell densities as well as the sugar concentrations, is illustrated to the right. The profile at time $t+1$ is obtained at the end of growth (row 4), and the entire cycle of dilution/migration and growth is repeated. As can be seen, after the completion of a cycle, the profile is shifted in space. At a given time t, the exact position of the wave is defined by the position at which the density profile crosses a certain threshold value (2000 cells, in the simulations). The velocity of expansion is given by the distance by which the profile shifts averaged over multiple cycles (bottom right).

Parameter	**Median**	**Literature**	**References**
Maximal growth rate on glucose, γ_{max} $[hr^{-1}]$	0.390	0.3 – 0.55 (0.39)	[50, 59, 13, 60]
K_M for growth on glucose, k_g [%W/V]	0.0019	0.002 – 0.003 (0.002)	[93]
K_M for sucrose hydrolysis, k_g [%W/V]	0.781	0.5 – 1.5 (0.8)	[59, 94, 92]
Maximal sucrose hydrolysis rate, v_s [%OD^{-1}hr^{-1}]	0.833	2.4 (2.4)	[59]
Privatization parameter, g_{eff} [OD hr]	0.02	0.0015 (0.0015)	[59]
Yield on glucose, Y [%OD^{-1}]	0.057	– (0.07)	–

Table A.1: The table shows a comparison between previously reported and median values of model parameters obtained by fitting the model to measured growth rates. Values in brackets under the literature column are used for the simulation in Figure A-7.

Appendix B

Appendix to chapter 3

B.1 Materials and methods

Strains

The expansion experiments were performed using two pairs of strains, BY-RFP/BY-YFP and DH-RFP/DH-CFP. The BY strains were derived from the haploid BY4741 strain (mating type **a**, EUROSCARF, CITE Jeff paper). The BY-YFP strain has a yellow fluorescent protein expressed constitutively by the ADH1 promoter (inserted using plasmid pRS401 containing MET17). The BY-RFP strain has a red fluorescent protein inserted into the HIS3 gene using plasmid pRS303. The DH strains are the same as those used in Healey et al (CITE). They are derived from the diploid strain W303, with the RFP/CFP strains harboring constitutively expressed fluorescent markers integrated into the URA3 gene. This pair is auxotrophic to uracil.

B.1.1 Growth rate measurements and calculation of Fisher velocities

Growth rates for both strain pairs were measured independently for all media, in growth conditions identical to the final expansion experiments. For each pair, the two fluorescent strains were mixed in 1:1 ratio in log phase and the cultures were diluted into a wide range ($10 cells/well$ to $10^5 cells/well$) of initial cell densities. They were then diluted 2x every 4 hours into fresh media. Initial and final densities of each fluorescent strain for each dilution cycle were measured using flow cytometry, and their growth rates as a function of cell density were derived from these measurements. The data is shown in SI. Low density growth rates were obtained by linear regression on the log of initial and final densities, for initial densities under $500 cells/well$. The Fisher velocities were then derived by simulating expansions with logistic growth, with the fitted low density growth rate. Uncertainty in Fisher velocities was obtained by bootstrapping.

B.1.2 Expansion experiment protocols

All experiments were performed at 30 in standard synthetic media (yeast nitrogen base and complete supplement mixture), in $200-\mu L$ batch culture in BD Biosciences Falcon 96-well Microtest plates. Expansions occurred along the 12 well long rows of the plate. Migrations and dilutions were performed every 4 h using the Tecan Freedom EVO 100 robot. Plates were not shaken during growth. Optical densities were measured on the robot before every dilution cycle in the Tecan Sunrise platereader with 600-nm light. Cell densities of individual fluorescent strains were also measured every 6 cycles in the MacsQuant flow cytometer after dilution in phosphate buffered saline (PBS). All expansions started with a steep exponential initial density profile. Periodically during the expansion, the leftmost well (in the bulk of the wave, away from the wavefront) was discarded and the entire profile was shifted to the left, so as to create empty wells for further expansion to the right. It was ensured that the rightmost two wells were always at zero cell density so as to avoid any edge effects on the expansion.

B.1.3 Definition of front

The 'front' is defined as the region of the wave density profile that fell below a threshold density, set at $0.2 \times N_{bulk}$. 'Fractions in the front' correspond to the fraction of fluorescent cells added up over the entire front region as defined above. The location of the front is defined as the interpolated well position where the density profile crosses the threshold.

B.2 Supplementary figures

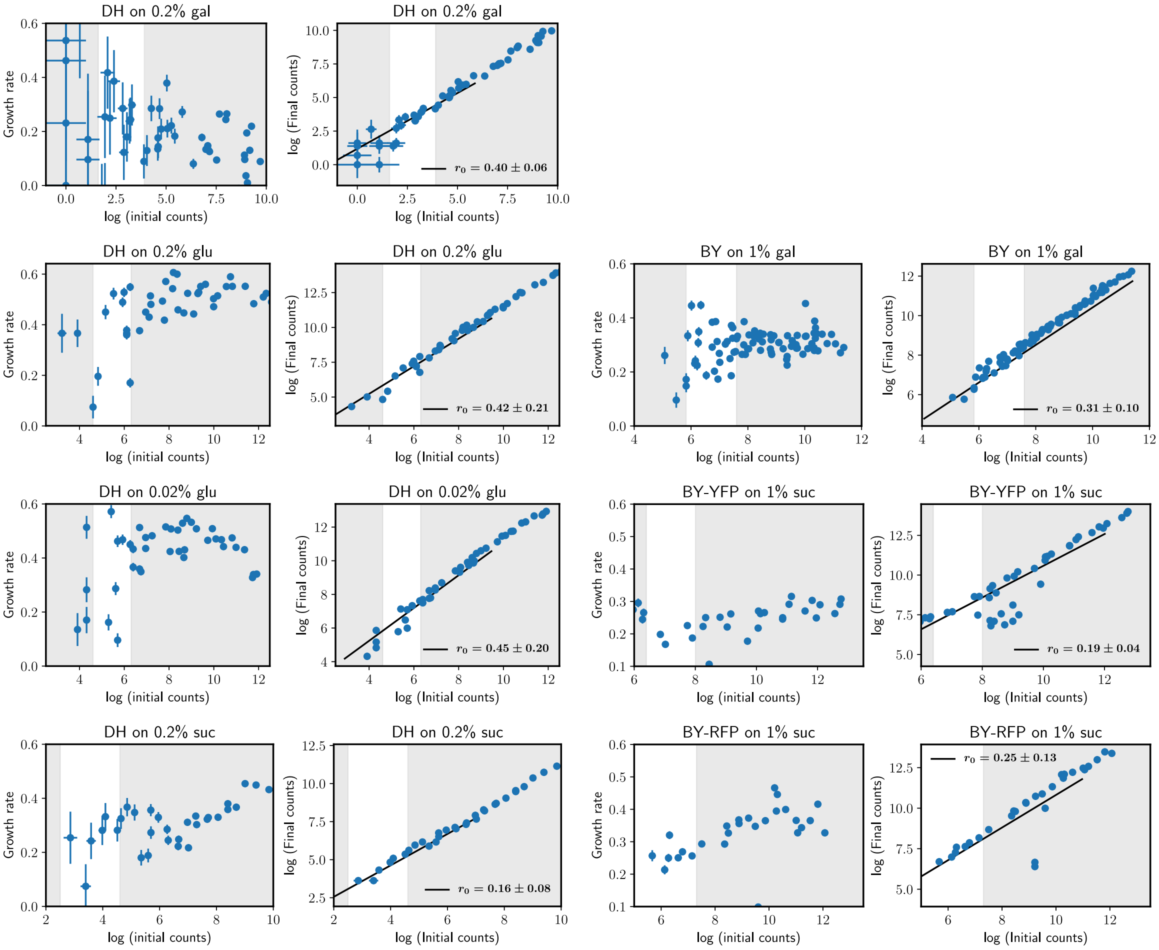

Figure B-1: Density dependence of growth and fits for low density growth rate for different strain-media combinations

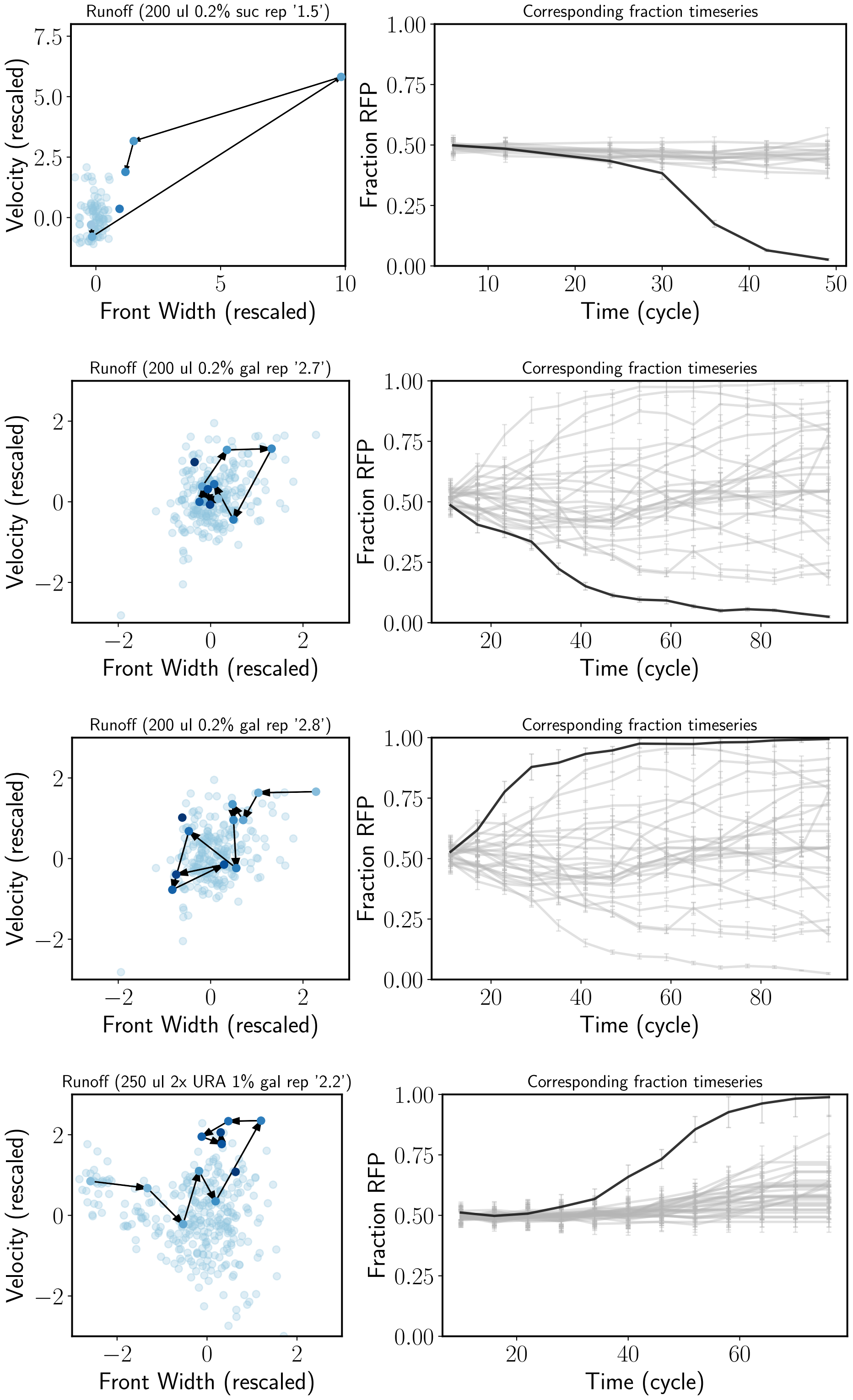

Figure B-2: Jackpots in experiments

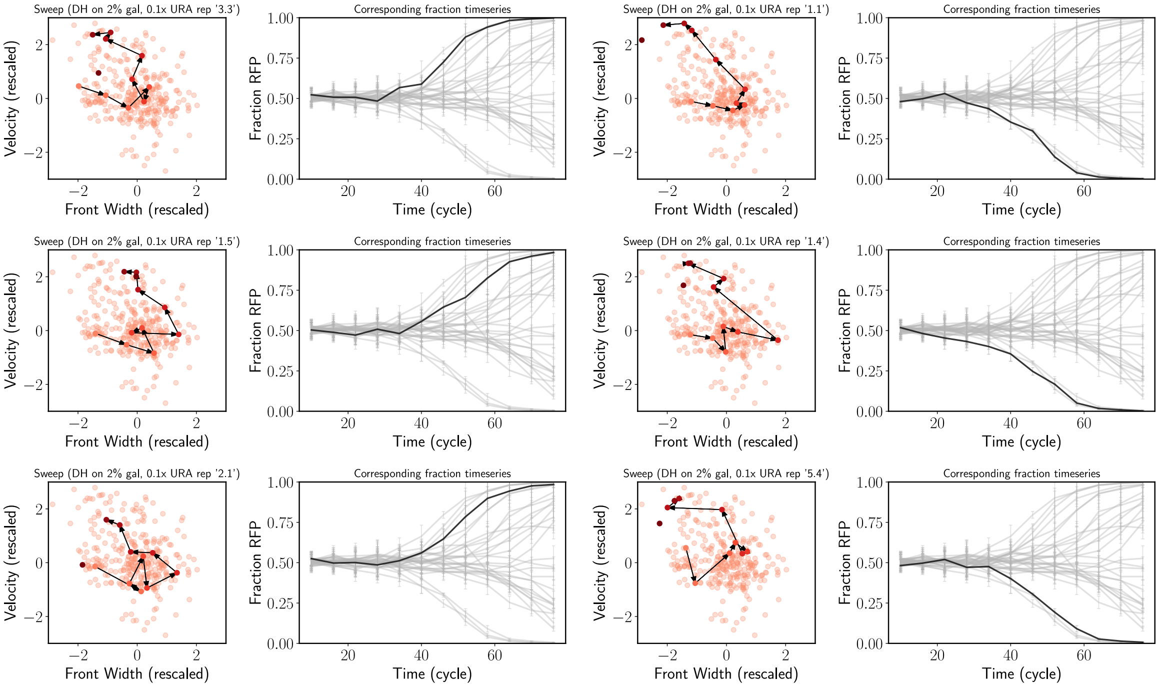

Figure B-3: All evolution state space diagrams

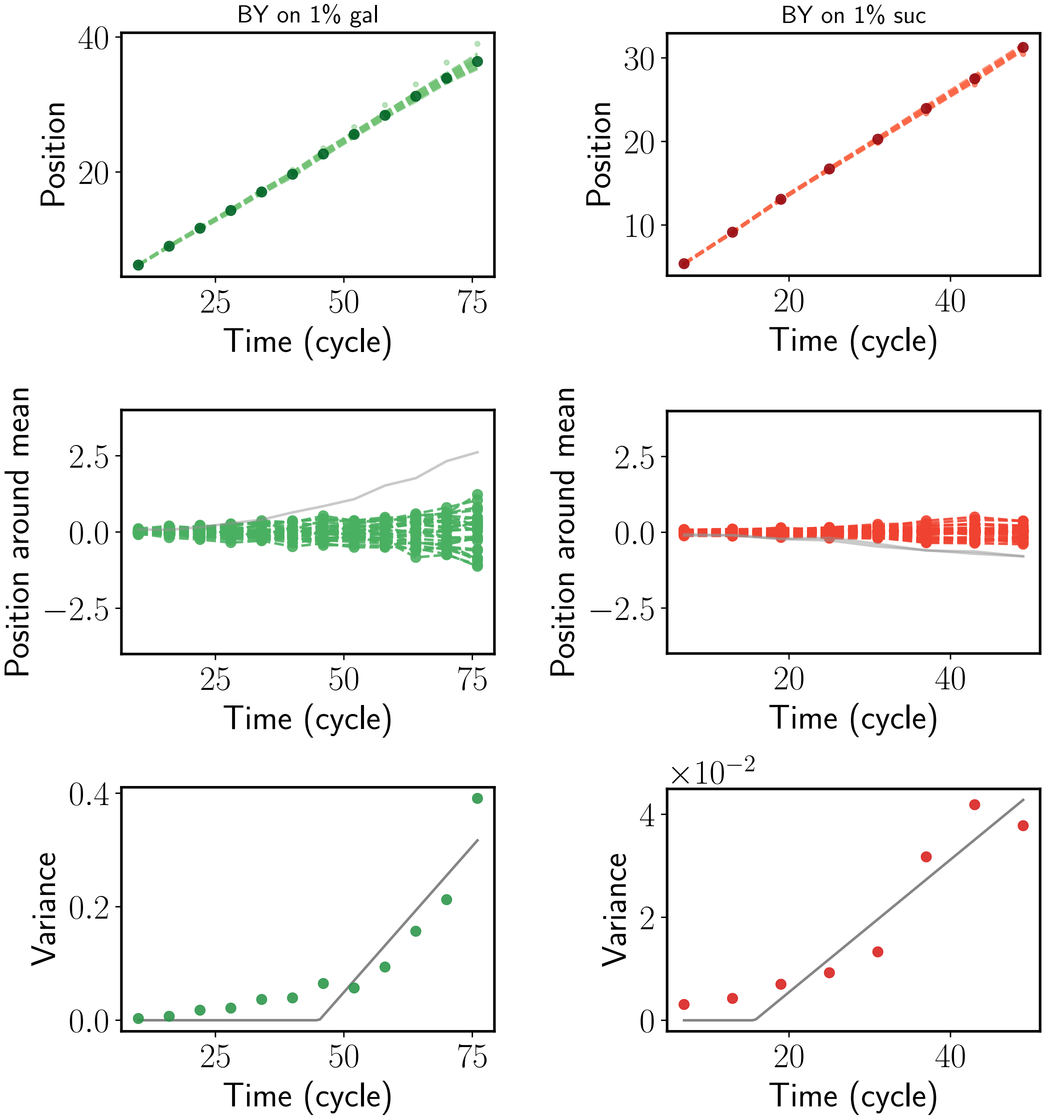

Figure B-4: Front diffusion figure

Strain, Media	**Growth Rates**	**Fisher Velocities (m, df)**
DH, 0.2% galactose	$0.4 \pm 0.06 hr^{-1}$	0.78 ± 0.12 $wells/cycle$ (0.4, 2)
DH, 0.2% glucose	$0.42 \pm 0.21 hr^{-1}$	0.60 ± 0.23 $wells/cycle$ (0.3, 2)
		0.72 ± 0.25 $wells/cycle$ (0.5, 2)
		0.70 ± 0.19 $wells/cycle$ (0.25, 1.33)
		0.64 ± 0.22 $wells/cycle$ (0.25, 1.54)
DH, 0.02% glucose	$0.45 \pm 0.2 hr^{-1}$	0.64 ± 0.26 $wells/cycle$ (0.4, 2)
DH, 0.2% sucrose	$0.16 \pm 0.08 hr^{-1}$	0.34 ± 0.16 $wells/cycle$ (0.4, 2)
BY, 1% galactose, 2x URA	$0.31 \pm 0.1 hr^{-1}$	0.51 ± 0.16 $wells/cycle$ (0.3, 2)
BY-YFP, 1% sucrose	$0.19 \pm 0.04 hr^{-1}$	0.30 ± 0.17 $wells/cycle$ (0.3, 2)
BY-RFP, 1% sucrose	$0.23 \pm 0.11 hr^{-1}$	0.37 ± 0.16 $wells/cycle$ (0.3, 2)

Table B.1: Growth rates and Fisher velocities of yeast strains in different growth media

Bibliography

[1] Michael J. Tyler. *Australian Frogs: A Natural History*. Cornell University Press, Ithaca, NY, December 1997.

[2] Benjamin L. Phillips, Gregory P. Brown, Jonathan K. Webb, and Richard Shine. Invasion and the evolution of speed in toads. *Nature*, 439(7078):803–803, February 2006.

[3] Benjamin L. Phillips, Gregory P. Brown, Matthew Greenlees, Jonathan K. Webb, and Richard Shine. Rapid expansion of the cane toad (Bufo marinus) invasion front in tropical Australia. *Austral Ecology*, 32(2):169–176, April 2007.

[4] Derek M. Johnson, Andrew M. Liebhold, Patrick C. Tobin, and Ottar N. Bjørnstad. Allee effects and pulsed invasion by the gypsy moth. *Nature*, 444(7117):361–363, November 2006.

[5] Andrew M. Liebhold, Joel A. Halverson, and Gregory A. Elmes. Gypsy Moth Invasion in North America: A Quantitative Analysis. *Journal of Biogeography*, 19(5):513–520, September 1992.

[6] Andrew M. Liebhold and Patrick C. Tobin. Growth of newly established alien populations: comparison of North American gypsy moth colonies with invasion theory. *Population Ecology*, 48(4):253–262, September 2006.

[7] Jonathan M. Levine and Carla M. D'Antonio. Forecasting Biological Invasions with Increasing International Trade. *Conservation Biology*, 17(1):322–326, February 2003.

[8] Godfrey Hewitt. The genetic legacy of the Quaternary ice ages. *Nature*, 405(6789):907–913, June 2000.

[9] Thomas Schmitt. Molecular biogeography of Europe: Pleistocene cycles and postglacial trends. *Frontiers in Zoology*, 4(1):11, April 2007.

[10] Stephen R. Keller, Matthew S. Olson, Salim Silim, William Schroeder, and Peter Tiffin. Genomic diversity, population structure, and migration following rapid range expansion in the Balsam Poplar, Populus balsamifera. *Molecular Ecology*, 19(6):1212–1226, March 2010.

[11] Shaoping Ling, Zheng Hu, Zuyu Yang, Fang Yang, Yawei Li, Pei Lin, Ke Chen, Lili Dong, Lihua Cao, Yong Tao, Lingtong Hao, Qingjian Chen, Qiang Gong, Dafei Wu, Wenjie Li, Wenming Zhao, Xiuyun Tian, Chunyi Hao, Eric A. Hungate, Daniel V. T. Catenacci, Richard R. Hudson, Wen-Hsiung Li, Xuemei Lu, and Chung-I Wu. Extremely high genetic diversity in a single tumor points to prevalence of non-Darwinian cell evolution. *Proceedings of the National Academy of Sciences of the United States of America*, 112(47):E6496–E6505, November 2015.

[12] S. Peischl, I. Dupanloup, M. Kirkpatrick, and L. Excoffier. On the accumulation of deleterious mutations during range expansions. *Molecular Ecology*, 22(24):5972–5982, December 2013.

[13] Lei Dai, Daan Vorselen, Kirill S. Korolev, and Jeff Gore. Generic Indicators for Loss of Resilience Before a Tipping Point Leading to Population Collapse. *Science*, 336(6085):1175–1177, June 2012.

[14] Timothy H. Keitt, Mark A. Lewis, and Robert D. Holt. Allee Effects, Invasion Pinning, and Species' Borders. *The American Naturalist*, 157(2):203–216, February 2001.

[15] M. C. Köhnke and H. Malchow. Wave pinning in competition-diffusion models in variable environments. *Journal of Theoretical Biology*, 461:204–214, January 2019.

[16] Saurabh R. Gandhi, Eugene Anatoly Yurtsev, Kirill S. Korolev, and Jeff Gore. Range expansions transition from pulled to pushed waves as growth becomes more cooperative in an experimental microbial population. *Proceedings of the National Academy of Sciences*, 113(25):6922–6927, June 2016.

[17] Eva Graciá, Andrés Giménez, José Daniel Anadón, D. James Harris, Uwe Fritz, and Francisco Botella. The uncertainty of Late Pleistocene range expansions in the western Mediterranean: a case study of the colonization of south-eastern Spain by the spur-thighed tortoise, Testudo graeca. *Journal of Biogeography*, 40(2):323–334, February 2013.

[18] Richard R. Veit and Mark A. Lewis. Dispersal, Population Growth, and the Allee Effect: Dynamics of the House Finch Invasion of Eastern North America. *The American Naturalist*, 148(2):255–274, August 1996.

[19] Rachel M. Pateman, Jane K. Hill, David B. Roy, Richard Fox, and Chris D. Thomas. Temperature-Dependent Alterations in Host Use Drive Rapid Range Expansion in a Butterfly. *Science*, 336(6084):1028–1030, May 2012.

[20] Gian-Reto Walther, Eric Post, Peter Convey, Annette Menzel, Camille Parmesan, Trevor J. C. Beebee, Jean-Marc Fromentin, Ove Hoegh-Guldberg, and Franz Bairlein. Ecological responses to recent climate change. *Nature*, 416(6879):389–395, March 2002.

[21] David Pimentel. *Biological Invasions: Economic and Environmental Costs of Alien Plant, Animal, and Microbe Species.* CRC Press, October 2014.

[22] Jefferson H. Mayo, Thomas J. Straka, and Donna S. Leonard. The Cost of Slowing the Spread of the Gypsy Moth (Lepidoptera: Lymantriidae). *Journal of Economic Entomology*, 96(5):1448–1454, October 2003.

[23] Robert W. Sutherst, Robert B. Floyd, and Gunter F. Maywald. The Potential Geographical Distribution of the Cane Toad, Bufo marinus L. in Australia. *Conservation Biology*, 10(1):294–299, February 1996.

[24] Brian Leung, John M. Drake, and David M. Lodge. Predicting invasions: propagule pressure and the gravity of allee effects. *Ecology*, 85(6):1651–1660, June 2004.

[25] Greta Bocedi, Stephen C.F. Palmer, Guy Pe'er, Risto K. Heikkinen, Yiannis G. Matsinos, Kevin Watts, and Justin M.J. Travis. RangeShifter: a platform for modelling spatial eco-evolutionary dynamics and species' responses to environmental changes. *Methods in Ecology and Evolution*, 5(4):388–396, April 2014.

[26] J. G. Skellam. Random Dispersal in Theoretical Populations. *Biometrika*, 38(1/2):196–218, June 1951.

[27] R. A. Fisher. The Wave of Advance of Advantageous Genes. *Annals of Eugenics*, 7(4):355–369, June 1937.

[28] Ilkka Hanski. *Metapopulation Ecology.* OUP Oxford, March 1999.

[29] Wim van Saarloos. Front propagation into unstable states. *Physics Reports*, 386(2–6):29–222, November 2003.

[30] J. D. Murray, editor. *Mathematical Biology*, volume 18 of *Interdisciplinary Applied Mathematics.* Springer-Verlag, New York, 1993.

[31] Franck Courchamp, Tim Clutton-Brock, Bryan Grenfell, Franck Courchamp, Tim Clutton-Brock, Bryan Grenfell, Franck Courchamp, Tim Clutton-Brock, Bryan Grenfell, Franck Courchamp, Tim Clutton-Brock, Bryan Grenfell, Franck Courchamp, Tim Clutton-Brock, and Bryan Grenfell. Inverse density dependence and the Allee effect. *Trends in Ecology & Evolution*, 14(10):405–410, January 1999.

[32] Warder Clyde Allee. *Principles of Animal Ecology.* Saunders Co., 1949.

[33] Andrew M. Kramer, Brian Dennis, Andrew M. Liebhold, and John M. Drake. The evidence for Allee effects. *Population Ecology*, 51(3):341–354, April 2009.

[34] P. A. Stephens, W. J. Sutherland, and R. P. Freckleton. What Is the Allee Effect? *Oikos*, 87(1):185–190, October 1999.

[35] Mark Kot. *Elements of Mathematical Ecology.* Cambridge University Press, July 2001.

[36] Oskar Hallatschek and David R. Nelson. Gene surfing in expanding populations. *Theoretical Population Biology*, 73(1):158–170, February 2008.

[37] K. S. Korolev, Mikkel Avlund, Oskar Hallatschek, and David R. Nelson. Genetic demixing and evolution in linear stepping stone models. *Reviews of modern physics*, 82(2):1691–1718, June 2010.

[38] Eva Graciá, Francisco Botella, José Daniel Anadón, Pim Edelaar, D. James Harris, and Andrés Giménez. Surfing in tortoises? Empirical signs of genetic structuring owing to range expansion. *Biology Letters*, 9(3):20121091, June 2013.

[39] Kris J. Hundertmark and Larry J. Van Daele. Founder effect and bottleneck signatures in an introduced, insular population of elk. *Conservation Genetics*, 11(1):139–147, November 2009.

[40] Sohini Ramachandran, Omkar Deshpande, Charles C. Roseman, Noah A. Rosenberg, Marcus W. Feldman, and L. Luca Cavalli-Sforza. Support from the relationship of genetic and geographic distance in human populations for a serial founder effect originating in Africa. *Proceedings of the National Academy of Sciences of the United States of America*, 102(44):15942–15947, November 2005.

[41] M. A. Lewis and P. Kareiva. Allee Dynamics and the Spread of Invading Organisms. *Theoretical Population Biology*, 43(2):141–158, April 1993.

[42] Brett A. Melbourne and Alan Hastings. Highly Variable Spread Rates in Replicated Biological Invasions: Fundamental Limits to Predictability. *Science*, 325(5947):1536–1539, September 2009.

[43] Jun-ichi Wakita, Kenji Komatsu, Akio Nakahara, Tohey Matsuyama, and Mitsugu Matsushita. Experimental Investigation on the Validity of Population Dynamics Approach to Bacterial Colony Formation. *Journal of the Physical Society of Japan*, 63(3):1205–1211, March 1994.

[44] Andrea Giometto, Andrea Rinaldo, Francesco Carrara, and Florian Altermatt. Emerging predictable features of replicated biological invasion fronts. *Proceedings of the National Academy of Sciences*, 111(1):297–301, January 2014.

[45] Christine M. Jessup, Rees Kassen, Samantha E. Forde, Ben Kerr, Angus Buckling, Paul B. Rainey, and Brendan J. M. Bohannan. Big questions, small worlds: microbial model systems in ecology. *Trends in Ecology & Evolution*, 19(4):189–197, April 2004.

[46] Babak Momeni, Kristen A. Brileya, Matthew W. Fields, and Wenying Shou. Strong inter-population cooperation leads to partner intermixing in microbial communities. *eLife*, 2:e00230, January 2013.

[47] Eshel Ben-Jacob, Inon Cohen, Ofer Shochet, Igor Aranson, Herbert Levine, and Lev Tsimring. Complex bacterial patterns. *Nature*, 373(6515):566–567, February 1995.

[48] S. J. Pirt. A Kinetic Study of the Mode of Growth of Surface Colonies of Bacteria and Fungi. *Journal of General Microbiology*, 47(2):181–197, May 1967.

[49] Kirill S. Korolev, Melanie J. I. Müller, Nilay Karahan, Andrew W. Murray, Oskar Hallatschek, and David R. Nelson. Selective sweeps in growing microbial colonies. *Physical Biology*, 9(2):026008, April 2012.

[50] Manoshi Sen Datta, Kirill S. Korolev, Ivana Cvijovic, Carmel Dudley, and Jeff Gore. Range expansion promotes cooperation in an experimental microbial metapopulation. *Proceedings of the National Academy of Sciences*, 110(18):7354–7359, April 2013.

[51] Kirill S. Korolev. The Fate of Cooperation during Range Expansions. *PLoS Comput Biol*, 9(3):e1002994, March 2013.

[52] Lin Chen, Javad Noorbakhsh, Rhys M. Adams, Joseph Samaniego-Evans, Germaine Agollah, Dmitry Nevozhay, Jennie Kuzdzal-Fick, Pankaj Mehta, and Gábor Balázsi. Two-Dimensionality of Yeast Colony Expansion Accompanied by Pattern Formation. *PLoS Comput Biol*, 10(12):e1003979, December 2014.

[53] J. David Van Dyken, Melanie J. I. Müller, Keenan M. L. Mack, and Michael M. Desai. Spatial Population Expansion Promotes the Evolution of Cooperation in an Experimental Prisoner's Dilemma. *Current Biology*, 23(10):919–923, May 2013.

[54] Markus F. Weber, Gabriele Poxleitner, Elke Hebisch, Erwin Frey, and Madeleine Opitz. Chemical warfare and survival strategies in bacterial range expansions. *Journal of The Royal Society Interface*, 11(96):20140172, July 2014.

[55] Benjamin Kerr, Margaret A. Riley, Marcus W. Feldman, and Brendan J. M. Bohannan. Local dispersal promotes biodiversity in a real-life game of rock–paper–scissors. *Nature*, 418(6894):171–174, July 2002.

[56] Oskar Hallatschek, Pascal Hersen, Sharad Ramanathan, and David R. Nelson. Genetic drift at expanding frontiers promotes gene segregation. *Proceedings of the National Academy of Sciences*, 104(50):19926–19930, December 2007.

[57] Kirill S. Korolev, João B. Xavier, David R. Nelson, and Kevin R. Foster. A Quantitative Test of Population Genetics Using Spatiogenetic Patterns in Bacterial Colonies. *The American Naturalist*, 178(4):538–552, October 2011.

[58] Caz M. Taylor and Alan Hastings. Allee effects in biological invasions. *Ecology Letters*, 8(8):895–908, August 2005.

[59] Jeff Gore, Hyun Youk, and Alexander van Oudenaarden. Snowdrift game dynamics and facultative cheating in yeast. *Nature*, 459(7244):253–256, May 2009.

[60] Alvaro Sanchez and Jeff Gore. Feedback between Population and Evolutionary Dynamics Determines the Fate of Social Microbial Populations. *PLoS Biol*, 11(4):e1001547, April 2013.

[61] John H. Koschwanez, Kevin R. Foster, and Andrew W. Murray. Sucrose Utilization in Budding Yeast as a Model for the Origin of Undifferentiated Multicellularity. *PLoS Biol*, 9(8):e1001122, August 2011.

[62] Éric Brunet and Bernard Derrida. Effect of Microscopic Noise on Front Propagation. *Journal of Statistical Physics*, 103(1-2):269–282, April 2001.

[63] Eric Brunet and Bernard Derrida. Shift in the velocity of a front due to a cutoff. *Physical Review E*, 56(3):2597–2604, September 1997.

[64] A.N. Kolmogorov, N Piscounov, and I Petrowski. Étude de l'équation de la diffusion avec croissance de la quantité de matière et son application a un problème biologique. *Moscow University Bulletin Of Mathematics*, 1:1–25, 1937.

[65] Lionel Roques, Jimmy Garnier, François Hamel, and Etienne K. Klein. Allee effect promotes diversity in traveling waves of colonization. *Proceedings of the National Academy of Sciences*, 109(23):8828–8833, June 2012.

[66] Patrick C. Tobin, Luděk Berec, and Andrew M. Liebhold. Exploiting Allee effects for managing biological invasions. *Ecology Letters*, 14(6):615–624, June 2011.

[67] Jintao Liu, Rosa Martinez-Corral, Arthur Prindle, Dong-yeon D. Lee, Joseph Larkin, Marçal Gabalda-Sagarra, Jordi Garcia-Ojalvo, and Gürol M. Süel. Coupling between distant biofilms and emergence of nutrient time-sharing. *Science (New York, N.Y.)*, 356(6338):638–642, May 2017.

[68] Antonio Brú, Sonia Albertos, José Luis Subiza, José López García-Asenjo, and Isabel Brú. The Universal Dynamics of Tumor Growth. *Biophysical Journal*, 85(5):2948–2961, November 2003.

[69] Dirk Brockmann and Dirk Helbing. The Hidden Geometry of Complex, Network-Driven Contagion Phenomena. *Science*, 342(6164):1337–1342, December 2013.

[70] Andrea R. Pluess. Pursuing glacier retreat: genetic structure of a rapidly expanding Larix decidua population. *Molecular Ecology*, 20(3):473–485, February 2011.

[71] Yvonne Willi, Josh Van Buskirk, and Ary A. Hoffmann. Limits to the Adaptive Potential of Small Populations. *Annual Review of Ecology, Evolution, and Systematics*, 37(1):433–458, 2006.

[72] Laurent Excoffier, Matthieu Foll, and Rémy J. Petit. Genetic Consequences of Range Expansions. *Annual Review of Ecology, Evolution, and Systematics*, 40(1):481–501, 2009.

[73] Montgomery Slatkin and Laurent Excoffier. Serial Founder Effects During Range Expansion: A Spatial Analog of Genetic Drift. *Genetics*, 191(1):171–181, May 2012.

[74] Lars Bosshard, Isabelle Dupanloup, Olivier Tenaillon, Rémy Bruggmann, Martin Ackermann, Stephan Peischl, and Laurent Excoffier. Accumulation of Deleterious Mutations During Bacterial Range Expansions. *Genetics*, 207(2):669–684, October 2017.

[75] Kimberly J. Gilbert, Stephan Peischl, and Laurent Excoffier. Mutation load dynamics during environmentally-driven range shifts. *PLOS Genetics*, 14(9):e1007450, September 2018.

[76] A. N. Stokes. On two types of moving front in quasilinear diffusion. *Mathematical Biosciences*, 31(3):307–315, January 1976.

[77] Franck Courchamp, Ludek Berec, and Joanna Gascoigne. *Allee Effects in Ecology and Conservation*. Oxford University Press, Oxford ; New York, April 2008.

[78] Jimmy Garnier and Mark A. Lewis. Expansion Under Climate Change: The Genetic Consequences. *Bulletin of Mathematical Biology*, 78(11):2165–2185, November 2016.

[79] Nathan G. Marculis, Roger Lui, and Mark A. Lewis. Neutral Genetic Patterns for Expanding Populations with Nonoverlapping Generations. *Bulletin of Mathematical Biology*, pages 1–25, March 2017.

[80] Devin W. Goodsman, Barry Cooke, David W. Coltman, and Mark A. Lewis. The genetic signature of rapid range expansions: How dispersal, growth and invasion speed impact heterozygosity and allele surfing. *Theoretical Population Biology*, 98:1–10, December 2014.

[81] Jimmy Garnier, Thomas Giletti, François Hamel, and Lionel Roques. Inside dynamics of pulled and pushed fronts. *Journal de Mathématiques Pures et Appliquées*, 98(4):428–449, October 2012.

[82] Gabriel Birzu, Oskar Hallatschek, and Kirill S. Korolev. Fluctuations uncover a distinct class of traveling waves. *Proceedings of the National Academy of Sciences*, 115(16):E3645–E3654, April 2018.

[83] R. Bialozyt, B. Ziegenhagen, and R. J. Petit. Contrasting effects of long distance seed dispersal on genetic diversity during range expansion. *Journal of Evolutionary Biology*, 19(1):12–20, January 2006.

[84] Susanne Lachmuth, Walter Durka, and Frank M. Schurr. The making of a rapid plant invader: genetic diversity and differentiation in the native and invaded range of Senecio inaequidens. *Molecular Ecology*, 19(18):3952–3967, September 2010.

[85] Daniel R. Amor, Raúl Montañez, Salva Duran-Nebreda, and Ricard Solé. Spatial dynamics of synthetic microbial mutualists and their parasites. *PLOS Computational Biology*, 13(8):e1005689, August 2017.

[86] Christoph Ratzke and Jeff Gore. Self-organized patchiness facilitates survival in a cooperatively growing *Bacillus subtilis* population. *Nature Microbiology*, 1(5):16022, May 2016.

[87] Shreyas Gokhale, Arolyn Conwill, Tanvi Ranjan, and Jeff Gore. Migration alters oscillatory dynamics and promotes survival in connected bacterial populations. *Nature Communications*, 9(1):5273, December 2018.

[88] E. Brunet, B. Derrida, A. H. Mueller, and S. Munier. Phenomenological theory giving the full statistics of the position of fluctuating pulled fronts. *Physical Review E*, 73(5):056126, May 2006.

[89] Christoph Ratzke and Jeff Gore. Modifying and reacting to the environmental pH can drive bacterial interactions. *PLOS Biology*, 16(3):e2004248, March 2018.

[90] Carl M. Bender and Steven A. Orszag. *Advanced Mathematical Methods for Scientists and Engineers I*. Springer New York, New York, NY, 1999.

[91] Mandisi Mrwebi. *Testing Monod : growth rate as a function of glucose concentration in Saccharomyces cerevisiae*. Thesis, Stellenbosch : University of Stellenbosch, December 2004.

[92] Antonio José Goulart, Andréa Francisco dos Santos, Olga Luisa Tavano, Julio Cesar Vinueza, Jonas Contiero, and Rubens Monti. Glucose and Fructose Production by Saccharomyces cerevisiae Invertase Immobilized on MANAE-Agarose Support. *Revista de Ciências Farmacêuticas Básica e Aplicada*, 34(2):169–175, June 2013.

[93] E. Ben-Jacob, H. Brand, G. Dee, L. Kramer, and J. S. Langer. Pattern propagation in nonlinear dissipative systems. *Physica D: Nonlinear Phenomena*, 14(3):348–364, March 1985.

[94] Michele Vitolo and Miriam T. Yassuda. Effect of sucrose concentration on the invertase activity of intact yeast cells (S. cerevisiae). *Biotechnology Letters*, 13(1):53–56, January 1991.